Dynamics of a distributed drill string system

Journal of Sound and Vibration 417 (2018) 376–412

Contents lists available at ScienceDirect

Journal of Sound and Vibration

journal homepage: www.elsevier.com/locate/jsvi

Dynamics of a distributed drill string system: Characteristic parameters and stability maps

Ulf Jakob F. Aarsnes [a,b,*], Nathan van de Wouw [c,d,e]

[a] International Research Institute of Stavanger (IRIS), Oslo, Norway
[b] DrillWell - Drilling and Well Centre for Improved Recovery, Stavanger, Norway
[c] Eindhoven University of Technology, Department of Mechanical Engineering, Eindhoven, The Netherlands
[d] Department of Civil, Environmental & Geo-Engineering, University of Minnesota, Minneapolis, USA
[e] Delft Center for Systems and Control, Delft University of Technology, Delft, The Netherlands

ARTICLE INFO

Article history:
Received 24 April 2017
Revised 30 November 2017
Accepted 1 December 2017
Available online 27 December 2017

Keywords:
Drill-string vibrations
Stick-slip
Distributed systems
Infinite dimensional systems
Stability
Delay equations

ABSTRACT

This paper involves the dynamic (stability) analysis of distributed drill-string systems. A minimal set of parameters characterizing the linearized, axial-torsional dynamics of a distributed drill string coupled through the bit-rock interaction is derived. This is found to correspond to five parameters for a simple drill string and eight parameters for a two-sectioned drill-string (e.g., corresponding to the pipe and collar sections of a drilling system). These dynamic characterizations are used to plot the *inverse gain margin* of the system, parametrized in the non-dimensional parameters, effectively creating a stability map covering the full range of realistic physical parameters. This analysis reveals a complex spectrum of dynamics not evident in stability analysis with lumped models, thus indicating the importance of analysis using distributed models. Moreover, it reveals trends concerning stability properties depending on key system parameters useful in the context of system and control design aiming at the mitigation of vibrations.

1. Introduction

The performance of rotary drilling systems used to drill boreholes in the earth is often limited by the occurrence of self-excited vibrations. Self-excited vibrations cause early fatigue of drill pipes and premature failure of bits and, therefore, should be avoided. Through a combination of damage to equipment, and increased downtime, drill string vibrations have been reported to account for 2–10% of well costs [1]. As fixed cutter bits (also known as PDC bits) are especially prone to self-excited vibrations, drilling systems employing these bits have seen significant scrutiny and attempts at mitigation of these vibrations.

To explain the occurrence of self-excited (axial and torsional) drill-string vibrations, a model of the relevant torsional and axial dynamics with an unstable equilibrium is needed. The implications of an equilibrium in this system being unstable is that a small initial perturbation to the system will grow over time and will, in severe cases, manifest itself as an observable oscillatory phenomena such as stick slip vibration or bit bouncing.

The cause of this instability in drilling systems with PDC bits have previously been explained by a rate-weakening effect[1] in the bit-rock interface law causing an instability in the torsional dynamics [2], and approaches to mitigating the oscillations by dealing with this instability directly started in the 90's [3,4]. Such approaches, although having been reasonably successful [5,6],

* Corresponding author. International Research Institute of Stavanger (IRIS), Forskningsparken AS, Gaustadalléen 21, 0349 Oslo, Norway.
E-mail addresses: ujfa@iris.no (U.J.F. Aarsnes), n.v.d.wouw@tue.nl (N. van de Wouw).

[1] Essentially a Stribeck-like effect.

https://doi.org/10.1016/j.jsv.2017.12.002
0022-460X/

Nomenclature

Independent variables

s	Laplace variable
t	Time in seconds
x	Axial position in meters

Independent variables

w	Force
τ	Torque
v	Axial velocity a delay differential equation which is in turn used to derive the minimal set of characteristic parameters that can be used to specify the linearized system dynamics. Based on the Nyquist criterion, the stability analysis is initiated in Section
ω	Angular velocity

Laplace transformed states *The subscripts $i \in \{0, b, p\}$ denotes 'top-drive', 'bit', and 'pipe-collar interface', respectively*

W_i	Weight
T_i	Torque
V_i	Axial velocity
Ω_i	Angular velocity

Drill string properties *The superscripts p, c denotes the pipe and collar section respectively*

A	Cross sectional area
E	Young's modulus
J	Polar moment of inertia
G	Shear modulus
ρ	Pipe density
k_a, k_t	Axial/torsional viscous damping coefficient

Bit rock interaction (BRI) parameters

a	Bit radius
ζ	Cutting force inclination
ϵ	Intrinsic specific rock energy
N	Number of cutters

Operational parameters

$\overline{v}$	Imposed steady-state axial velocity
$\overline{\omega}$	Imposed steady-state angular velocity

Non-dimensional characteristic quantities, for $i \in \{a, t\}$ (axial,torsional)

$\eta_i = -k_i^d k_i^L$	Pseudo reflection coefficient
$\overline{K}_i = t_* K_i$	Nominal loop gain
$\overline{\Omega} = 1/\overline{t}_N = \frac{t_* N}{2\pi}\overline{\omega}$	Steady-state angular velocity
$\overline{c} = \frac{c_a}{c_t} \approx 1.6$	Relative wave speeds
$\overline{\zeta}_i = \frac{\zeta_i^c}{\zeta_i^p}$	Relative collar to pipe impedance
$\eta_i^c = \frac{1-\overline{\zeta}_i}{1+\overline{\zeta}_i} e^{-k_i^c t_i^c}$	Collar section psuedo reflection coefficient
$\overline{t}_p = \frac{t_t^p}{t_*} = \frac{L^p}{L^p+L^c}$	Drill pipe travel time

Non-dimensional independent variables, with $t_* = t_t L/c_t$

$\overline{s} = s t_* = \mathrm{j}\varpi$	Dimensionless Laplace variable
ϖ	Dimensionless frequency variable

Derived quantities, for $i \in \{a, t\}$ ***(axial, torsional)***

$t_N = \frac{\overline{v}}{N\overline{\omega}}$	Steady-state BRI delay
$\zeta_i = \frac{AE}{c_a}, \frac{JG}{c_t}$	Axial/torsional impedance
$\zeta_i^p = \frac{A^pE^p}{c_a}, \frac{J^pG^p}{c_t}$	Pipe axial/torsional impedance
$\zeta_i^c = \frac{A^cE^c}{c_a}, \frac{J^cG^c}{c_t}$	Pipe axial/torsional impedance
$c_i = \sqrt{\frac{E}{\rho}}, \sqrt{\frac{G}{\rho}}$	Axial/torsional, wave speed
$t_i = \frac{L}{c_i}$	Axial, torsional, travel time
$t_i^c = \frac{L^c}{c_i}$	Collar section Axial/torsional travel time
$t_i^p = \frac{L^p}{c_i}$	Pipe section Axial/torsional travel time
$K_a = \frac{a\zeta\epsilon N}{\zeta_a}, \frac{a\zeta\epsilon N}{\zeta_a^c}$	Nominal axial loop gain single-section/two-section
$K_t = \frac{\overline{v}}{\overline{\omega}}\frac{a^2\epsilon N}{2\zeta_t}, \frac{\overline{v}}{\overline{\omega}}\frac{a^2\epsilon N}{2\zeta_t^c}$	Nominal torsional loop gain single-section/two-section
$k_i^d = e^{-2k_it_i}$	In-domain damping coefficient
$k_i^L = \frac{\zeta_i - Z_i^L}{\zeta_i + Z_i^L}, \frac{\zeta_i^p - Z_i^L}{\zeta_i^p + Z_i^L}$	Reflection coefficient single-section/two-section
$M_{G,i} = \max_{\varpi\in\varpi_{180}} \left\lvert \frac{\overline{G}_i(\mathrm{j}\varpi)}{\overline{K}_i} \right\rvert$	Normalized inverse gain margin
$\varpi_{180} = \{\varpi \in \mathbb{R} : \angle\overline{G}_i(\mathrm{j}\varpi) = 180°\}$	Set of frequencies $\overline{G}_i(s)$ crosses 180°

Transfer functions, for $i \in \{a, t\}$ ***(axial,torsional)***

$Z_i(s) = \zeta_i\left(1 + \frac{k_i}{s}\right)^{1/2}$	Characteristic line impedance
$Z_i^p(s) = \zeta_i^p\left(1 + \frac{k_i}{s}\right)^{1/2}$	Pipe section, characteristic line impedance
$Z_i^c(s) = \zeta_i^c\left(1 + \frac{k_i}{s}\right)^{1/2}$	Collar section, characteristic line impedance
$Z_i^L(s) = -\frac{W_0}{V_0}(s), -\frac{T_0}{\Omega_0}(s)$	Load impedance
$\Gamma_i(s) = st_i\left(1 + \frac{k_i}{s}\right)^{1/2}$	Propagation operator
$\Gamma_i^p(s) = st_i^p\left(1 + \frac{k_i}{s}\right)^{1/2}$	Propagation operator, collar section
$\Gamma_i^c(s) = st_i^c\left(1 + \frac{k_i}{s}\right)^{1/2}$	Propagation operator, collar section
$g_i(s) = -\zeta_a\frac{V_b}{W_b}, -\zeta_t\frac{\Omega_b}{T_b}$	Drill-string transfer function, single-section case
$g_i^p(s) = -\zeta_a^p\frac{V_p}{W_p}, -\zeta_t^p\frac{\Omega_p}{T_p}$	Pipe-section transfer function
$g_i^c(s) = -\zeta_c^p\frac{V_b}{W_b}, -\zeta_t^c\frac{\Omega_b}{T_b}$	Drill-string transfer function, two-section case
$D(s) = \frac{N}{s}\left[V_b(s)\left(1 - e^{-t_Ns}\right) - \frac{\overline{v}}{\overline{\omega}}\Omega_b(s)\left(1 - e^{-t_Ns}\right)\right]$	Combined depth of cut
$G(s) = G_a(s) + G_t(s)$	Loop transfer function
$G_i(s)$	Axial/torsional loop transfer function

Non-dimensional equivalents

$\overline{G}_i(st_*) = G_i(s)$ Axial/torsional loop transfer function

$\overline{g}_i(st_*) = g_i(s)$ Drill-string transfer function, single-section case

is still an active field of ongoing research [7–11].

At the same time, there has been continued research into the underlying causes of the instabilities, and recent results point to a more nuanced explanation: Models with a rate-independent bit-rock interaction law have been found to predict self-excited vibrations, including stick-slip, through the so-called regenerative effect [12], also well known in the literature on tool chatter in metal machining [13,14]. This effect introduces a *feedback* in the system, as the current force on the bit, which is a function of the instantaneous depth of cut, depends on the axial position of the bit at an earlier time [15,16]. This feedback may cause

instability depending on the dynamic response of the drill string. Furthermore, experiments with single cutters does not reveal any intrinsic velocity weakening effect [17], which seems to discount the explanation of the inherent rate weakening effect in the bit-rock interaction as the root cause for stick-slip vibrations.

Instead, in Ref. [12], it is proposed that the observed decrease in torque on bit at increasing rotational speeds is, as stated by Ref. [18], "likely to be the result of complex drill string dynamics rather than an intrinsic property of the bit-rock interaction" and in Ref. [19] it is stated that "the apparent decrease of the mean torque with the angular velocity responsible for the growth of the amplitude of the torsional vibrations is a consequence of the axial vibrations."

That is to say, the rate-(or velocity-) weakening effect can still be viewed as the cause of the torsional stick-slip limit cycle, but it is not an inherent property of the bit-rock interaction law, but rather a symptom of an axial limit-cycle caused by an axial instability through the regenerative effect. Hence, the axial instability is intimately linked to the observable, and unwanted, torsional stick-slip oscillations. In fact, previous publications, including [18,20,21], have posited that avoiding the axial instability could effectively remove the rate-weakening effect causing the torsional stick slip oscillations as well. Whether, and how, the axial instability can be removed is, however, as of yet undecided.

The current paper intends to present a structured investigation into the local stability properties of the axial and torsional dynamics of a distributed drill string coupled with a rate-independent bit-rock interaction law. In particular, we investigate the potential instability as caused by the regenerative effect of the bit rock interaction. We will consider linearized mathematical models and perform stability analyses to characterize the local dynamics close to a nominal equilibrium; herewith, insights are obtained into for which operating conditions drill-string vibrations are eminent. Consequently, as well as providing novel dynamic analysis results, a key 'stepping stone result' of the present study is in parameterizing the distributed system with a minimal set of parametric quantities, hereby providing, firstly, a suitable model for parameter stability analysis and, secondly, a modeling framework for future simulation studies that will be required to investigate the non-local dynamics of the system.

This work builds on and extends the developments in Ref. [22], where the bit-rock interaction proposed in Ref. [12] is combined with an infinite-dimensional (wave equation) description of the drill-string dynamics to arrive at a frequency-domain stability analysis result. The main novel contributions of the current paper are:

- Firstly, the decomposition of the systems characteristic equation (determining stability) into scaled non-dimensional factors with clearly defined impact on the dynamics (formulated in the frequency domain), herein including the effect of the parameters in the bit-rock interaction law and the geometry of the drill string. Using non-dimensional quantities, we obtain a minimal set of parameters to describe the system dynamics of a single section and a one- and two-section drill string, easing the subsequent analysis.
- Secondly, we introduce the inverse gain margin of the system. This enables determining the margin of stability or instability, parametrized in the loop gain coefficient which is key in determining stability, and which is determined partly by uncertain bit-rock interaction parameters.
- Thirdly, the inverse gain margin is plotted, parameterized in the previously obtained non-dimensional quantities, creating stability maps covering all possible sets of parameters of a two-sectioned drill string.
- Finally, these stability maps are analyzed to extract key features of the dynamics. Specifically, our results confirms previous observations that reducing the reflection of incoming waves at the top-drive, and increasing the top-drive RPM, both have stabilizing effects. Additionally, for the two-section drill string, we observe a complex interaction between the drill-string dynamics and the bit-rock interaction delay, which can significantly affect the severity of the axial instability (compared to the case of a single-section drill-string).

By pin-pointing the key factors contributing to severity and existence of axial and torsional drill-string instabilities (as caused by the regenerative effect), and providing a tool for quantifying the (lack of) stability properties, the proposed model and analysis results have significant potential for improving the design of drilling systems.

The outline of the present work is as follows. First, in Section 2, we derive the full linearized model describing the distributed drill string–bit-rock interaction system. Section 3 proposes an approximation of the system model in terms of a delay differential equation which is in turn used to derive the minimal set of characteristic parameters that can be used to specify the linearized system dynamics. Based on the Nyquist criterion, the stability analysis is initiated in Section 4 where we argue that the axial and torsional dynamics can be considered in isolation and derive conservative sufficient conditions for stability. Then, in Section 5 presents the stability maps covering the full range realistic parameters for the drill string system, before a usage of these is illustrated in Section 6. Finally, based on the preceding, conclusions are drawn in Section 7.

2. Model description

This section derives the mathematical description of the dynamics of the drilling system shown schematically in Fig. 1. We start by introducing the wave equation, describing the axial and torsional dynamics of the drill string from first principles, and then derive the corresponding transfer function using a transmission line description. The linearized Laplace transformed bit-rock interaction law is also given, which together with the wave equation of the drill string gives a complete description of model to be analyzed.

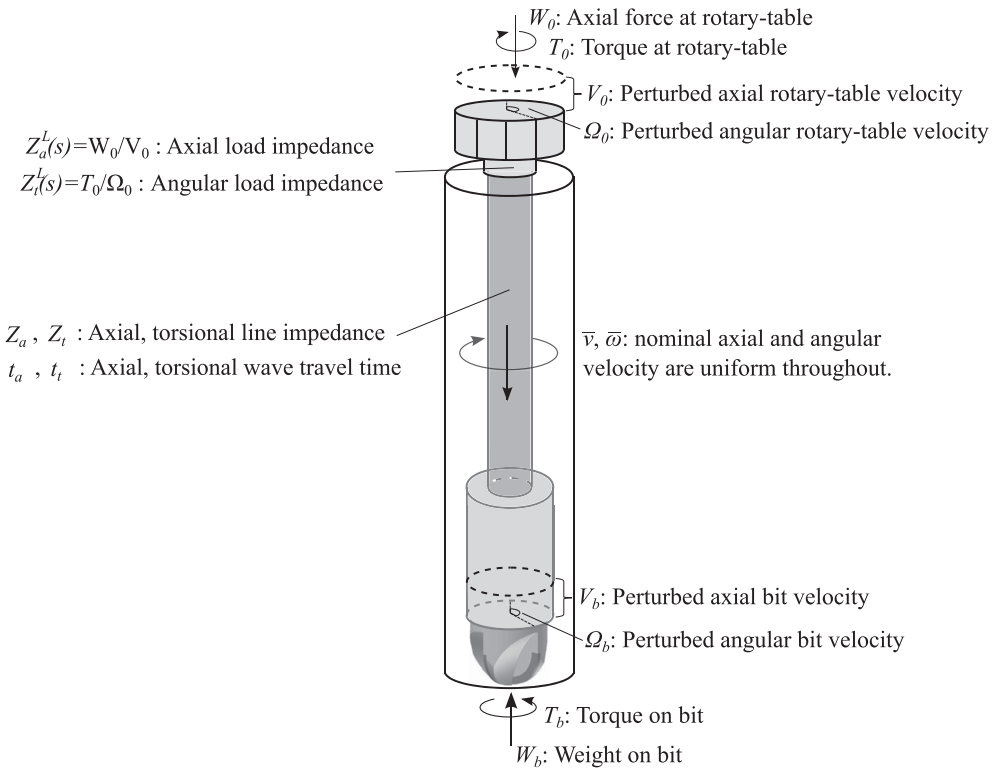

Fig. 1. Schematic of the drill string.

2.1. Axial and torsional dynamics of the drill string

2.1.1. Wave equation model

The dynamics of interest can be derived by assuming elastic deformations and using equations of continuity and state and the momentum balance acting on an infinitesimal drill string element. We refer to [22] for details of the derivation. Denoting the axial velocity and force by $v(t,x)$, $w(t,x)$, respectively, where $(t,x) \in [0,\infty) \times [0,L]$, with L the length of the drill-string, the axial dynamics are given as

$$\frac{\partial w(t,x)}{\partial t} + AE\frac{\partial v(t,x)}{\partial x} = 0 \tag{1}$$

$$A\rho\frac{\partial v(t,x)}{\partial t} + \frac{\partial w(t,x)}{\partial x} = -k_a\rho A v(t,x), \tag{2}$$

where A is the cross sectional area of the element and E is the Young's modulus and ρ is the pipe mass density and k_a is a damping constant representing the shear stresses and structural damping. Equivalently, for the angular motion, we denote the angular velocity and torque as $\omega(t,x)$, $\tau(t,x)$, respectively, with $(t,x) \in [0,\infty) \times [0,L]$, the angular dynamics are given as

$$\frac{\partial \tau(t,x)}{\partial t} + JG\frac{\partial \omega(t,x)}{\partial x} = 0 \tag{3}$$

$$J\rho\frac{\partial \omega(t,x)}{\partial t} + \frac{\partial \tau(t,x)}{\partial x} = -k_t\rho J\omega(t,x), \tag{4}$$

where J is the polar moment for inertia and G is the shear modulus and k_t is a damping constant representing the combined effect of shear stresses and structural damping.

2.1.2. Transmission line model

The following derivation of a transmission line model formulation resembles what is known as the transfer matrix approach [23–25], which is an effective way to capture the distributed dynamics inherent in a long drill-string [15,26].[2]

Define the axial and torsional wave velocities $c_a = \sqrt{E/\rho}$, $c_t = \sqrt{G/\rho}$; then, the characteristic line impedances Z_i, $i \in \{a,t\}$, and propagation operators, Γ_i, $i \in \{a,t\}$, for (1)–(4), respectively, are given as

$$Z_a(s) = \zeta_a\left(1+\frac{k_a}{s}\right)^{1/2}, \quad \Gamma_a(s) = st_a\left(1+\frac{k_a}{s}\right)^{1/2}, \quad \text{with} \quad \zeta_a \equiv \frac{AE}{c_a} = A\rho c_a, \quad t_a = \frac{L}{c_a}, \tag{5}$$

$$Z_t(s) = \zeta_t\left(1+\frac{k_t}{s}\right)^{1/2}, \quad \Gamma_t(s) = st_t\left(1+\frac{k_t}{s}\right)^{1/2}, \quad \text{with} \quad \zeta_t \equiv \frac{JG}{c_t} = J\rho c_t, \quad t_t = \frac{L}{c_t}. \tag{6}$$

where t_i, $i \in \{a,t\}$, is the transport delay of the wave equation, i.e., the time it takes the wave to travel one length of the drill-string, and ζ_i, $i \in \{a,t\}$, is a characteristic quantity determining the magnitude of the impedance of the drill string. Now the axial and torsional distributed systems both satisfy the well-known closed form general solution of transmission lines which can be given as a two-port configuration [27,28]:

$$\begin{bmatrix} W_b(s) \\ V_b(s) \end{bmatrix} = \begin{bmatrix} \cosh\Gamma_a & -Z_a\sinh\Gamma_a \\ -\frac{1}{Z_a}\sinh\Gamma_a & \cosh\Gamma_a \end{bmatrix}\begin{bmatrix} W_0(s) \\ V_0(s) \end{bmatrix}, \quad \begin{bmatrix} T_b(s) \\ \Omega_b(s) \end{bmatrix} = \begin{bmatrix} \cosh\Gamma_t & -Z_t\sinh\Gamma_t \\ -\frac{1}{Z_t}\sinh\Gamma_t & \cosh\Gamma_t \end{bmatrix}\begin{bmatrix} T_0(s) \\ \Omega_0(s) \end{bmatrix}, \tag{7}$$

where the subscripts b, 0 denote the bit and topside locations, respectively, i.e., $W_b(s) = W(s, x = L)$ and $W_0(s) = W(s, x = 0)$, see Fig. 1.

As the topside boundary, we need expressions relating the axial velocity to force, and the angular velocity to torque. If such relations can be specified as a Linear Time Invariant (LTI) system (e.g., a controller) mapping velocity to force/torque then these can be described by their Laplace transforms and we will denote the resulting transfer functions as $Z_a^L(s), Z_t^L(s)$, respectively, for the axial and torsional boundary conditions. That is, we can write

$$Z_a^L(s) \equiv -\frac{W_0(s)}{V_0(s)}, \quad Z_t^L(s) \equiv -\frac{T_0(s)}{\Omega_0(s)}. \tag{8}$$

Note that the load impedance formulation of (8) is quite general and allows for any linear dynamic relation between the forces/torques and velocities, including dynamic controller formulations such as [7,10,21], Soft Torque [6] and impedance matching [29].

For cases when no active controllers are applied, the load impedance can typically be approximated with a constant, i.e. $Z^L(s) = Z^L$, to ease analysis.

The linear axial and torsional drill string dynamics are described by the non-dimensional transfer functions $g_a(s), g_t(s)$, respectively. These transfer functions can be found by combining (7) and (8). For the axial dynamics, $g_a(s)$ relates weight on bit W_b to axial bit velocity V_b as follows:

$$\frac{V_b}{W_b}(s) \equiv -\frac{1}{\zeta_a}g_a(s), \quad g_a(s) = \frac{\zeta_a}{Z_a}\frac{Z_a + Z_a^L\tanh\Gamma_a}{Z_a^L + Z_a\tanh\Gamma_a}, \tag{9}$$

while for the torsional dynamics $g_t(s)$ relates torque on bit T_b to angular bit velocity Ω_b as follows:

$$\frac{\Omega_b}{T_b}(s) \equiv -\frac{1}{\zeta_t}g_t(s), \quad g_t(s) = \frac{\zeta_t}{Z_t}\frac{Z_t + Z_t^L\tanh\Gamma_t}{Z_t^L + Z_t\tanh\Gamma_t}, \tag{10}$$

where we have normalized the functions $g_a(s), g_t(s)$ to make these dimensionless.

2.2. Two section drill-string

For a typical realistic drilling system the lower-most section of the drill-string consist of series of thick pipes called drill collars. The resulting discontinuity in inertia causes reflections in the torsional and axial waves of the system which have significant impact on the dynamics.

Considering a drill string with two sections, we will refer to the lower-most section as the *drill collar* and associated parameters will be indicated with the superscript c. Correspondingly, the top-most section will be referred to as the *drill pipe*, connected to the drill collar at the bottom and the load impedance Z_i^L at the top, and will be denoted with the superscript p, see Fig. 2.

[2] Note that, although the notation is similar to that of [22], we use force and torque instead of axial and angular strain, resulting in different characteristic line impedances. This change in model formulation is to simplify the later analysis when extending the model to incorporate multiple drill-string sections (e.g., such as the drill pipe section and the bottom-hole assembly section with distinct piping geometries).

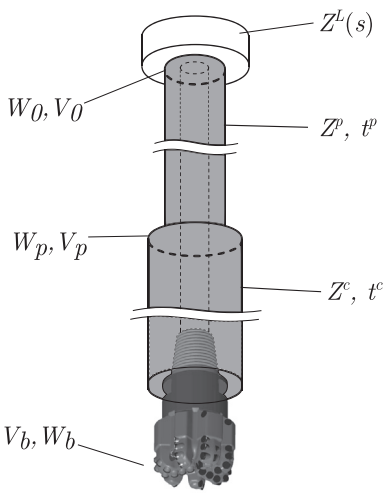

Fig. 2. Two-sectioned drill string schematic.

To derive the transfer function for this case, recall the two-port configuration of (7) which can now be applied to both the drill collar and the drill pipe. For the axial dynamics, by combining two such transfer matrices we obtain

$$\begin{bmatrix} W_b(s) \\ V_b(s) \end{bmatrix} = \begin{bmatrix} \cosh\,\Gamma_a^c & -Z_a^c\,\sinh\,\Gamma_a^c \\ -\frac{1}{Z_a^c}\sinh\,\Gamma_a^c & \cosh\,\Gamma_a^c \end{bmatrix} \begin{bmatrix} \cosh\,\Gamma_a^p & -Z_a^p\,\sinh\,\Gamma_a^p \\ -\frac{1}{Z_a^p}\sinh\,\Gamma_a^p & \cosh\,\Gamma_a^p \end{bmatrix} \begin{bmatrix} W_0(s) \\ V_0(s) \end{bmatrix}. \tag{11}$$

This relation can also be derived by first finding the relation between force and velocity at the transition, $W_p(s)$, $V_p(s)$, and using this as the load impedance for the collar section. I.e., the load seen from the collar section is, using the definition (8):

$$-\frac{W_p}{V_p} \equiv \frac{\zeta_a^p}{g_a^p(s)}, \qquad g_a^p(s) = \frac{\zeta_a^p}{Z_a^p}\frac{Z_a^p + Z_a^L\,\tanh\,\Gamma_a^p}{Z_a^L + Z_a^p\,\tanh\,\Gamma_a^p}, \tag{12}$$

see Fig. 2 for notation. Then we can write the transfer function of the two section drill string as

$$\frac{V_b}{W_b} = -\frac{1}{\zeta_a^c} g_a^c(s) = -\frac{1}{Z_a^c}\frac{Z_a^c + \frac{\zeta_a^p}{g_a^p(s)}\tanh\,\Gamma_a^c}{\frac{\zeta_a^p}{g_a^p(s)} + Z_a^c\,\tanh\,\Gamma_a^c}. \tag{13}$$

A similar relation as in (11) and (13) can be obtained for the torsional dynamics, but is omitted here for the sake of brevity.

2.3. Bit-rock interaction law

We adopt the bit-rock interaction law of [30], which is a nonlinear relation that can include both cutting and frictional effects [15]. Since we pursue a (local) stability analysis, however, we are only interested in perturbed displacements from a nominal equilibrium and the resulting state-dependent (perturbed) forces, i.e., we use the first-order approximation of the bit-rock interaction law valid close to the equilibrium corresponding to a constant and non-zero axial and torsional velocity. Hence we discard the non-linear and static part of the bit-rock interaction equations and write perturbed weight and torque on bit as, following (see Fig. 3) [12,15]:

$$W_b(s) = a\zeta\epsilon D(s), \quad T_b(s) = \frac{1}{2}a^2\epsilon D(s), \tag{14}$$

where ϵ is the intrinsic specific energy of the rock, ζ is a number characterizing the inclination of the cutting force and a is the bit radius. Finally, $D(s)$ is Laplace transform of the combined depth of cut which, when linearized (see e.g. Refs. [12,13,16]), can

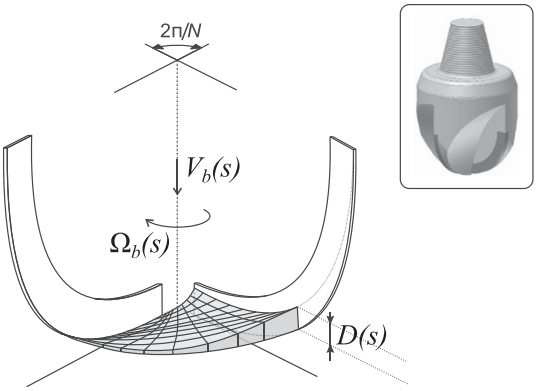

Fig. 3. Downhole bit-rock interaction. Adapted from Refs. [12,15].

be written as [22]:

$$D(s) = \frac{N}{s}\left[V_b(s)\left(1 - e^{-t_N s}\right) - \frac{\overline{v}}{\overline{\omega}}\Omega_b(s)\left(1 - e^{-t_N s}\right)\right], \tag{15}$$

where N is the number of blades on the PDC bit, the equilibrium rate-of-penetration (ROP) is denoted by $\overline{v}$ and the equilibrium angular velocity (RPM) is denoted by $\overline{\omega}$. Finally, $t_N = \frac{2\pi}{N\overline{\omega}}$ is the (constant) time between two successive cutters passing the same angular position at the equilibrium angular velocity $\overline{\omega}$.

2.4. Full model

The complete Laplace transformed linear perturbation dynamics of the drill-string is given by (9), (10), (14), (15). This set of equations are represented as a block diagram in Fig. 4. Considering Fig. 4, the two feedback loops, which can cause instability, are clearly identified. As shown in Ref. [22], the stability of this feedback system can be assessed by employing a version of the Nyquist stability criterion to check for the presence of right-half plane poles of the system. Specifically the occurrence of an instability of system (9), (10), (14), (15) (where $g_t(s), g_a(s)$ can denote any stable and proper transfer function) coincides with the existence of zeros in the Right Half Plane (RHP) of the system's characteristic equation:

$$G(s) + 1 = 0, \tag{16}$$

where

$$G(s) = G_a(s) + G_t(s), \tag{17}$$

$$G_a(s) = g_a(s)\frac{K_a}{s}\left(1 - e^{-t_N s}\right), \tag{18}$$

$$G_t(s) = -g_t(s)\frac{K_t}{s}\left(1 - e^{-t_N s}\right). \tag{19}$$

$$K_a = \frac{a\zeta\epsilon N}{\zeta_a}, \quad K_t = \frac{\overline{v}}{\overline{\omega}}\frac{a^2\epsilon N}{2\zeta_t}. \tag{20}$$

This characteristic equation can be found by solving for the system of Eqs. (9), (10), (14), (15), (also see Ref. [22]). This system is depicted in block diagram form in Fig. 4. The characteristic equation will be explored in detail in the scope of stability analysis in Section 4.1.

3. Parametric characterization of the drill-string dynamics

In this section, we parametrize the drill string transfer functions $g_a(s), g_t(s)$ in terms of a set of characteristic quantities. A step towards this goal is the approximation of the wave equation as a delay system, as presented in Section 3.1. This enables an intuitive understanding of the dynamics and allows for simpler approximations of the involved transfer functions. The time-domain version of these delay equations will not be used in the present note.

Subsequently, we use such model approximations to characterize the dynamics in $g_i(s)$, $i \in \{a, t\}$, in terms of a minimal set of parameters in Section 3.2. This is done for a single section drill-string in Section 3.2.1 and for a two-sectioned drill-string in Section 3.2.2. We also show in the latter two sections how these characteristic parameters determine key properties of the

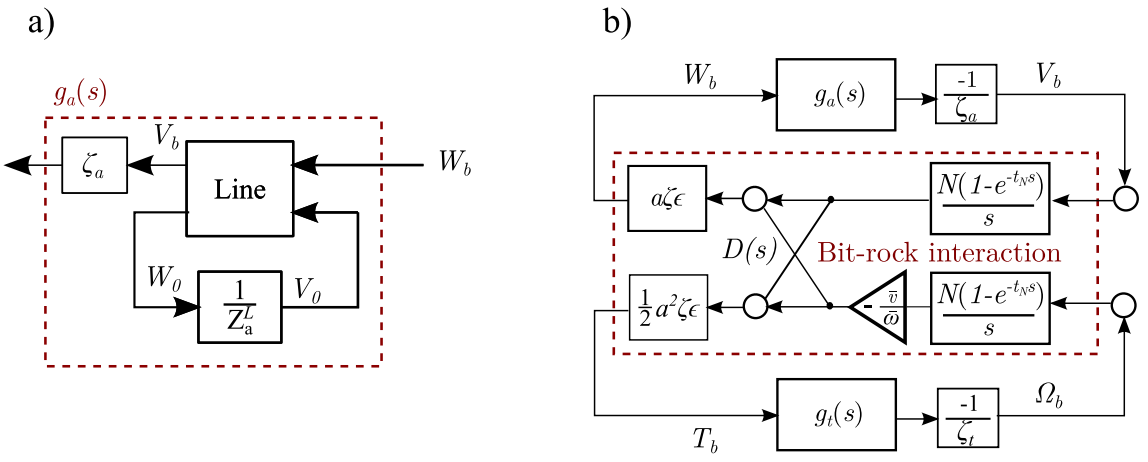

Fig. 4. Block diagram of $g_a(s)$ (left), and the full interconnected system (right). The block diagram $g_t(s)$ is equivalent to that of $g_a(s)$. The 'Line' block denotes a transformed version of the 2×2 port system of (7). Adapted from Ref. [22].

drillstring dynamics characterized in $g_i(j\omega)$, $i \in \{a, t\}$, such as the location of the resonances and anti-resonances in $g_i(j\omega)$, and the related magnitudes of $g_i(j\omega)$ at these (anti-) resonances, and the related phase properties. The obtained insights will prove to be instrumental in the analysis of stability properties performed in Sections 4 and 5.

Throughout this section, when the subscript i is used, it can be used to indicate a or t, for the axial or torsional derivation, respectively. This is due to the fact that, since the torsional and axial dynamics have a similar structure, the results are equivalent and hold for both cases.

3.1. Model approximation using delay equations

Define the Riemann invariants

$$\alpha_a = v + \frac{1}{\zeta_a} w, \quad \beta_a = v - \frac{1}{\zeta_a} w, \tag{21}$$

or, for the case of torsional dynamics,

$$\alpha_t = \omega + \frac{1}{\zeta_t} \tau, \quad \beta_t = \omega - \frac{1}{\zeta_t} \tau. \tag{22}$$

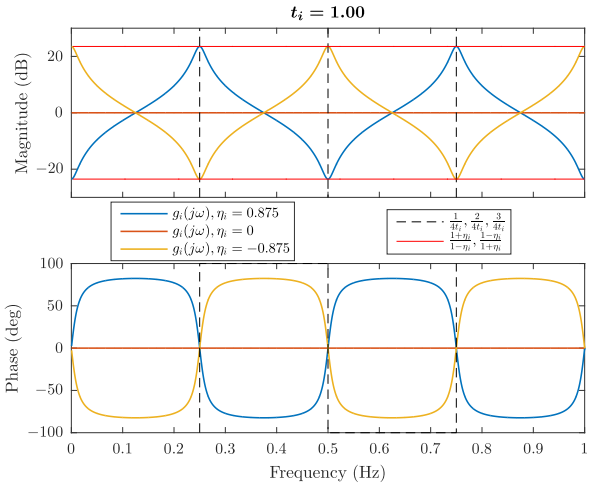

Fig. 5. Bode plot of $g_i(j\omega)$, for different topside loads characterized by η_i, and with $k_i = 0$. The interpretation of the influence of the characteristic parameters η_i, t_i on $g_i(s)$ are indicated. Note how the magnitude of $g_i(j\omega)$ is contained to a band around 1 (i.e., magnitude of 0 dB and phase of 0°), where the resonances are located according to the delay t_i and with a magnitude characterized by η_i.

Using the coordinate transform (21), or (22) for the torsional case, the partial differential equations (1) and (2), or (3) and (4), can be expressed with the variables $\alpha_i, \beta_i, \quad i \in \{a, t\}$, as the diagonalized partial differential equations

$$\frac{\partial \alpha_i}{\partial t} + c_i \frac{\partial \alpha_i}{\partial x} = -k_i(\beta_i + \alpha_i) \tag{23}$$

$$\frac{\partial \beta_i}{\partial t} - c_i \frac{\partial \beta_i}{\partial x} = -k_i(\beta_i + \alpha_i). \tag{24}$$

To avoid the in-domain coupling between the Riemann invariants, and enable the solutions at the boundary to be expressed in closed form as delay equations we approximate (23) and (24) as follows:

$$\frac{\partial \alpha_i}{\partial t} + c_i \frac{\partial \alpha_i}{\partial x} = -k_i \alpha_i \tag{25}$$

$$\frac{\partial \beta_i}{\partial t} - c_i \frac{\partial \beta_i}{\partial x} = -k_i \beta_i. \tag{26}$$

This is a reasonable approximation when the solutions of $\alpha_i, \beta_i, \quad i \in \{a, t\}$, does not have a significant static component, as can be seen in Fig. A.27 in Appendix A. This is true in our case as we are concerned with perturbation dynamics. Now it is straight forward to solve (25) and (26) (e.g., using the method of characteristics [31]) to arrive at the relations

$$\alpha_i(t, x = L) = \sqrt{k_i^d}\, \alpha_i(t - t_i, x = 0) \tag{27}$$

$$\beta_i(t, x = 0) = \sqrt{k_i^d}\, \beta_i(t - t_i, x = L), \tag{28}$$

where we have defined the variable $k_i^d = e^{-2k_i t_i}$ representing the in-domain damping.

Assuming a static boundary condition at the top drive, i.e., of the form $W_0 = Z_a^L V_0$, and writing:

$$\alpha_i(t, x = 0) \equiv k_i^L \beta_i(t, x = 0) \tag{29}$$

we can insert (21) or (22) into (29) to arrive at the reflection coefficient k_i^L given by

$$k_i^L = \frac{\zeta_i - Z_i^L}{\zeta_i + Z_i^L}. \tag{30}$$

Here, we observe that there is no reflection when $Z_i^L = \zeta_i$, which is a well-known phenomenon of transmission lines [32] as this correspond to impedance matching as seen from the approximation $Z_i(s) \approx \zeta_i$ (see (5), (6)).

Now, by combining (28), (29) and (27) we arrive at the relation

$$\alpha(t, L) = -\eta_i \beta(t - 2t_i, L), \tag{31}$$

where $\eta_i \equiv -k_i^d k_i^L$ is the product of the damping in the domain and at the topside boundary. Thus, by using the transformation (21) we obtain the following approximative axial dynamics:

$$v(t, L) + \frac{1}{\zeta_a} w(t, L) = \eta_a \left(v\left(t - 2t_a, L\right) - \frac{1}{\zeta_a} w\left(t - 2t_a, L\right) \right). \tag{32}$$

Using the subscript $_b$ to denote the downhole location at the bit at $x = L$, we write the relation between axial force at bit and velocity at bit in terms of a delay equation as follows:

$$v_b(t) - \eta_a v_b(t - 2t_a) = -\frac{1}{\zeta_a} \left[w_b(t) + \eta_a w_b(t - 2t_a) \right], \tag{33}$$

An evaluation of the accuracy of this approximation is given in Appendix A (see Fig. A.27). An equivalent expression for the torsional dynamics can be derived but is omitted here for the sake of brevity.

3.2. Characteristic system parameters

Recall the characteristic equation for evaluating (in)stability, $1 + G_a(s) + G_t(s)$, see (17), with the axial and torsional terms, respectively, given by

$$G_a(s) = g_a(s) \frac{K_a}{s} \left(1 - e^{-t_N s}\right), \quad K_a = \frac{a \zeta \epsilon N}{\zeta_a}, \tag{34}$$

$$G_t(s) = -g_t(s) \frac{K_t}{s} \left(1 - e^{-t_N s}\right), \quad K_t = \frac{\overline{v}}{\overline{\omega}} \frac{a^2 \epsilon N}{2\zeta_t}. \tag{35}$$

where $a \in [0.1, 0.3]$(m) is the bit radius, $\zeta \in [0.5, 0.8]$ is dependent on cutter sharpness [33], $\epsilon \in [20, 100] * 10^6$(Pa) is the intrinsic specific energy [34], N is the number of blades on the bit, $\frac{\overline{v}}{\overline{\omega}} \in [0.3, 3] * 10^{-3} \left(\frac{\text{m}}{\text{rad}}\right)$ is the ratio of axial to angular equilibrium velocity and $\zeta_a \in [0.1, 1] * 10^6 \left(\frac{\text{N}}{\text{m/s}}\right)$, $\zeta_t \in [0.2, 2] * 10^3 \left(\frac{\text{N}}{\text{m/s}}\right)$, where *typical* parameter ranges have been indicated.

To ease stability analysis, we will reduce the number of parameters by introducing dimensionless parameters. Define the characteristic quantity $t_* = t_t = \frac{L}{c_t}$ and correspondingly dimensionless time as $\overline{t} = t/t_*$. We use t_* to make the transfer function dimensionless by defining the Laplace variable $\overline{s} = st_*$. Note how this also implies the dimensionless steady-state angular velocity $\overline{\Omega} = \frac{t_* N}{2\pi}\overline{\omega}$, such that the we can express the terms of the characteristic equations in (34) and (35) as

$$\overline{G}_a(\overline{s}) = \overline{g}_a(\overline{s})\frac{\overline{K}_a}{\overline{s}}\left(1 - e^{-\overline{s}/\overline{\Omega}}\right), \quad \overline{K}_a = \frac{a\zeta\epsilon N t_*}{\zeta_a}, \tag{36}$$

$$\overline{G}_t(\overline{s}) = -\overline{g}_t(\overline{s})\frac{\overline{K}_t}{\overline{s}}\left(1 - e^{-\overline{s}/\overline{\Omega}}\right), \quad \overline{K}_t = \frac{\overline{v}}{\overline{\omega}}\frac{a^2\epsilon N t_*}{2\zeta_t}, \tag{37}$$

where $\overline{g}_i(st_*) \equiv g_i(s)$.

3.2.1. Characteristic parameters for a single section drill string

Considering the approximations $\frac{V_b(s)}{W_b(s)} \approx -\frac{1}{\zeta_a}\hat{g}_a(s)$ and $\frac{\Omega_b(s)}{T_b(s)} \approx -\frac{1}{\zeta_t}\hat{g}_t(s)$, where

$$\hat{g}_i(s) = \frac{1 - \eta_i e^{-s2t_i}}{1 + \eta_i e^{-s2t_i}}, \quad i \in \{a, t\}, \tag{38}$$

(see Appendix A) it is clear that the distributed drill-string transfer function relating the bit velocity to the weight on bit is determined by the following three parameters:

- ζ_i – gives the nominal magnitude of the drill string response,
- t_i – wave travel time in seconds, the inverse of which gives the frequency of the (anti-) resonances,
- $\eta_i = \frac{Z_i^L - \zeta_i}{Z_i^L + \zeta_i} e^{-2k_i t_i} \in [-1, 1]$, a pseudo-reflection coefficient which gives an approximate supremum of the magnitude of the transfer function (at the resonances), i.e.:

$$|g_i(s)|_\infty \approx \frac{1 + |\eta_i|}{1 - |\eta_i|}, \tag{39}$$

  and accounts for the damping at the boundary and the viscous damping in the domain. Note the singularity when $\eta = \pm 1$, which corresponds to cases without any damping in the system (similar to the transfer function of an oscillator without damping).

The effect of these characteristic parameters are shown in Fig. 5. The scaling ζ_i, which makes the transfer function $g_i(s)$ non-dimensional, also ensure the normalization $g_i(s) \approx 1$ for $\eta_i = 0$, see Fig. 5.

The complete (scaled) single-section drill-string–bit-rock interaction system, given by (37), (36), (9), (10) is specified by the following dimensionless parameters:

- $\overline{\Omega} = \frac{t_* N}{2\pi}\overline{\omega}$ - Dimensionless top-drive RPM, given as angular velocity relative to the drill string travel time. Determines the nominal delay in the bit rock interaction delay term.
- $\overline{K}_a = K_a t_*$ - Nominal axial loop gain coefficient, determined by bit-rock interaction and drill string parameters.
- $\overline{K}_t = K_t t_*$ - Nominal torsional loop gain coefficient, determined by bit-rock interaction and drill string parameters, and the axial to angular velocity ration.
- η_a, η_t - Pseudo reflection coefficient, given by the amount of damping in the system.
- $\overline{c} = \frac{c_a}{c_t} = \frac{t_t}{t_a} \approx 1.6$ - Relative magnitude of the axial and torsional wave speeds.

3.2.2. Characteristic parameters for a two-section drill string

For the case of a drill string with two-sections the associated transfer function $g_i(s)$, derived in (11), shown in Fig. 6, is significantly more complex and the details of its analysis is relegated to Appendix C. There we characterize the resonance frequencies and the associated magnitude by means of a key set of parameters in the spirit of Section 3.2.1.

Here, we summarize the set of characteristic quantities that can be used to parameterize a dimensionless model of a two sectioned drill string system.

Define the characteristic quantity $t_* = t_t^p + t_t^c$ and correspondingly non-dimensional time as $\overline{t} = t/t_*$. For the two section case, the drill string transfer function $g_a(s)$ in $\frac{V_b(s)}{W_b(s)} = \frac{-1}{\zeta_a}g_a(s)$, or $g_t(s)$ in $\frac{\Omega_b(s)}{T_b(s)} = \frac{-1}{\zeta_t}g_t(s)$, is obtained from (11), (8), and can be characterized by four parameters:

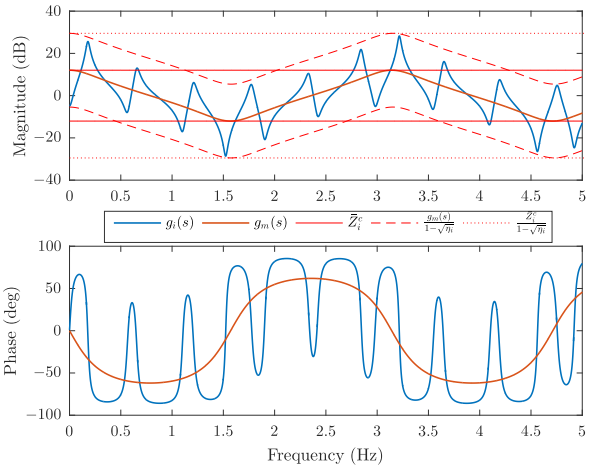

Fig. 6. Bode plot of $g_i(s)$ for a two sectioned pipe, showing $g_i(s)$ together with the case with matched load ($g_m(s)$) and worst-case resonant gain limits. The limits are shown with their inverses also plotted. Characteristic parameter used are $\overline{Z}_i^c *= 4$, $\eta_i = 0.75$, $\overline{t}_p = 0.84$ and the travel time is $t_* = 1$ seconds.

- $\overline{\zeta}_i = \frac{\zeta_i^c}{\zeta_i^p}$: relative magnitude of collar and pipe impedance. This parameter determines the location of resonances and anti-resonances, as given by (C.7)–(C.8) and determines the magnitude of the resonances of $g_m(s)$ as stated in the point below.
- $\eta_i^c = \frac{1-\overline{\zeta}_i}{1+\overline{\zeta}_i} e^{-k_i^c t_i^c} \in [-1, 1]$: determines the magnitude of the resonances of $g_m(s)$. Note that this implies the bound

$$\frac{1+|\eta_i^c|}{1-|\eta_i^c|} = \frac{1+\left|\frac{1-\overline{\zeta}_i}{1+\overline{\zeta}_i} e^{-k_i^c t_i^c}\right|}{1-\left|\frac{1-\overline{\zeta}_i}{1+\overline{\zeta}_i} e^{-k_i^c t_i^c}\right|} < \overline{\zeta}_i. \tag{40}$$

- $\eta_i = \frac{Z_i^L-\zeta_i^p}{Z_i^L+\zeta_i^p} e^{-k_i^c t_i^c - k_i^p t_i^p} \in [-1, 1]$: determines, together with η_i^c, the magnitude of the resonances of $g_i(s)$.
- $\overline{t}_p = \frac{t_t^p}{t_*} \in [0, 1]$: drill pipe travel time. Note that this implies $\overline{t}^c = 1 - \overline{t}_p$.

Remark 1. In most realistic cases the in-domain dissipation term in η_i^c is insignificant compared to the effect of the change in impedance, represented by $\overline{Z}_i^c$, hence it is amenable to describe the two section drill string transfer functions, $g_a(s)$ and $g_t(s)$, by only the five parameters $\overline{\zeta}_a, \overline{\zeta}_t, \eta_a, \eta_t, \overline{t}_p$.

In summary, employing the previous remark and assuming $\overline{c} = 1.6$ as set, by adding the parameters of the bit rock interaction (summarized in Section 3.2.1), the complete two-section drill-string–bit-rock interaction system can be specified by the eight dimensionless parameters: $\overline{\zeta}_i, \eta_i, \overline{K}_i$ for $i \in \{a, t\}$, and $\overline{t}_p, \overline{\Omega}$.

3.3. Typical parameter ranges

The dimensionless loop gain coefficients $\overline{K}_a, \overline{K}_t$ plays key roles in determining stability of the system. It should be noted that $\overline{K}_a, \overline{K}_t$ are proportional to the length of the well, L, through the characteristic time t_*, see (36). For the typical parameter ranges given above, we find the range $\overline{K}_a \in [3, 1000]t_*$, while $\overline{K}_t \in [0.05, 250]t_*$.

Meanwhile, the dimensionless top-drive RPM have a typical range of $\overline{\Omega} = [0.4, 4]t_*$, for the pseudo reflection coefficient we expect values in the range $\eta_i \in \pm[0.6, 0.9]$, $i \in \{a, t\}$, relative impedance $\overline{\zeta}_i^c \in [1, 10]$ $i \in \{a, t\}$ and for the characteristic time we obtain the range $t_* \in [0.1, 2](s)$.

3.4. Relation to lumped-parameter models in the literature

It is instructive to consider how the distributed model formulation compares to the lumped models of previous papers on this topic. Retaining the notation where the drill string transfer function is denoted by $g_i(s)$, $i \in \{a, t\}$, some of the models employed in previous literature is summarized in Table 1.

Of particular interest is the relation to the seminal RGD model due to [12]. In Appendix B it is shown that the RGD model can be obtained as an approximation of a system with a collar section that is infinitely *dense* and *short* and with a relatively short

Table 1
Table of some axial and torsional Transfer Functions used in the literature.

Literature reference	$\frac{V_b}{W_b} = -\frac{1}{\zeta_a} g_a(s)$	$\frac{\Omega_b}{T_b} = -\frac{1}{\zeta_t} g_t(s)$
Two-section distributed	$\frac{1}{\zeta_a^c} \frac{g_a^p(s)\zeta_a^c + \zeta_a^p \tanh s\frac{t^c}{\bar{c}}}{\zeta_a^p + \zeta_a^c g_a^p(s) \tanh s\frac{t^c}{\bar{c}}}$	$\frac{1}{\zeta_t^c} \frac{g_t^p(s)\zeta_t^c + \zeta_t^p \tanh st^c}{\zeta_t^p + \zeta_t^c g_t^p(s) \tanh st^c}$
[16]	$\frac{1}{M} \frac{s}{s^2 + sk_a + \frac{C_a}{M}}$	$\frac{1}{I} \frac{s}{s^2 + sk_t + \frac{C_t}{I}}$
[18]	$\frac{1}{M} \frac{s}{s^2 + sk_a + \frac{C_a}{M}}$	$\frac{1}{I} \frac{s}{s^2 + \frac{C_t}{I}}$
[12,35]	$\frac{1}{M} \frac{1}{s}$	$\frac{1}{I} \frac{s}{s^2 + \frac{C_t}{I}}$

pipe section. That is, the RGD model is an amenable approximation when:

$$t^c \frac{\varpi}{t_*} \ll 1, \qquad \text{for lumping the collar section.} \tag{41}$$

$$\frac{\zeta_a^p \varpi}{t_* M} \ll \frac{1 + |\eta_a|}{1 - |\eta_a|}, \quad \text{for discarding the pipe section.} \tag{42}$$

The above considerations also highlight when the RGD model is not a suitable approximation of the drill-string dynamics.

4. Simplifying heuristics and remarks on the stability result

In this section, we restate the stability result of [22] and investigate its implications. Our main approach is to develop heuristics which approximately correspond to the stability result of Theorem 1, below, but which are easier to grasp the practical ramifications of, as pertaining to a physical drilling system.

4.1. The Nyquist stability criterion

Recall the characteristic equation stated in (17), which we now consider in non-dimensional form

$$\overline{G}(\bar{s}) + 1 = 0, \quad \overline{G}(\bar{s}) = \overline{G}_a(\bar{s}) + \overline{G}_t(\bar{s}), \tag{43}$$

where

$$\overline{G}_a(\bar{s}) = \overline{g}_a(\bar{s}) \frac{\overline{K}_a}{\bar{s}} \left(1 - e^{-\bar{s}/\overline{\Omega}}\right), \quad \overline{G}_t(\bar{s}) = -\overline{g}_t(\bar{s}) \frac{\overline{K}_t}{\bar{s}} \left(1 - e^{-\bar{s}/\overline{\Omega}}\right). \tag{44}$$

This characteristic equation can be found by solving for the system of Eqs. (9), (10), (14), (15), (also see Ref. [22]). This system is depicted in block-diagram form in Fig. 4.

$\overline{G}(\bar{s})$ consists of two terms due to the two feedback loops seen in Fig. 4: an axial term $\overline{G}_a(\bar{s})$ and a torsional term $\overline{G}_t(\bar{s})$, which correspond to the axial and torsional *loop transfer functions*, respectively. Each of the terms can be split up into three non-dimensional factors. For the axial term, these three factors are: $\overline{g}_a(\bar{s})$ which represents the response of the drill string, $\overline{K}_a/\bar{s}$ a gain factor, and finally the delay factor $1 - e^{-\bar{s}/\overline{\Omega}}$ due to the bit-rock interaction. A similar decomposition holds for $\overline{G}_t(\bar{s})$, see (19).

Stability can be assessed by application of the Nyquist criterion, which is based on Cauchy's integral theorem [36], as summarized in the following theorem.

Theorem 1. *Suppose that $\overline{g}_a(\bar{s})$ and $\overline{g}_t(\bar{s})$ are stable transfer functions and denote the Nyquist contour of $\overline{G}(\bar{s})$ by $\Gamma_{\overline{G}(\bar{s})}$. Then, the system given by the* equations (9)–(15) *is*

- ***Unstable*** *if $\Gamma_{\overline{G}(\bar{s})}$ encircles -1.*
- ***Asymptotically stable*** *if $\Gamma_{\overline{G}(\bar{s})}$ does not encircle and does not cross -1.*

In the limiting case that $\Gamma_{\overline{G}(\bar{s})}$ does not encircle but crosses -1, the stability is undetermined.

Proof. The proof is given in [22]. □

By Nyquist contour, $\Gamma_{\overline{G}(\bar{s})}$, we mean the line that is created as $\overline{G}(\bar{s})$ is evaluated along the imaginary axis: $\bar{s} = \mathrm{j}\varpi, \quad \varpi \in (-\infty, \infty)$, and this criterion is typically checked graphically through the use of a Nyquist or Nichols diagram.

Remark 2. Parallels of this theorem can clearly be drawn to classical usage of the Nyquist stability criterion applied to a systems' loop transfer function. Indeed, by inspecting the considered systems block diagram, shown in Fig. 4, $\overline{G}(\bar{s})$ can be seen to be the loop transfer function obtained by opening the loops at the input ports to the bit-rock interaction.

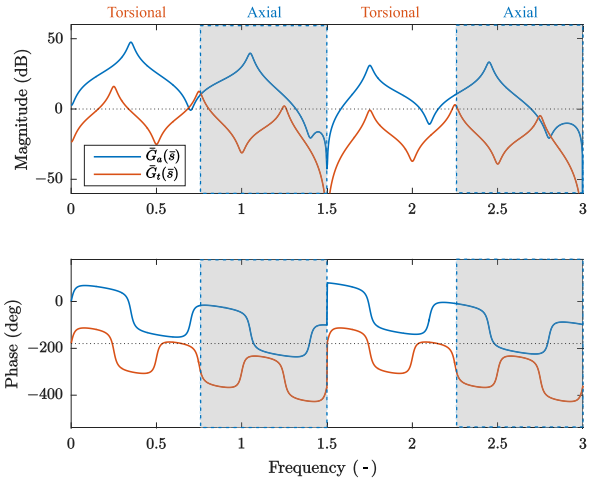

Fig. 7. Bode diagram of the "open loop" axial and torsional subsystems $\overline{G}_a(\bar{s}), \overline{G}_t(\bar{s})$. The torsional, respectively axial, term can only cross 180° (and cause instability) when the delay phase contribution is positive, respectively, negative (indicated in gray). Parameters $K_a = 20, K_t = 1, \overline{\Omega} = 1.5, \eta_a = \eta_t = 0.82, \overline{c} = 1.4$.

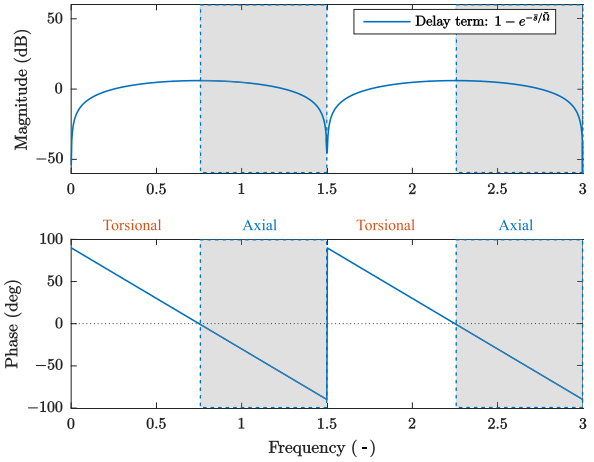

Fig. 8. Bode diagram of the delay term (right). The regions where the delay factor has a negative phase contribution is indicated in gray. Parameter $\overline{\Omega} = 1.5$.

A slightly conservative restatement of the result in Theorem 1 is the following: If there does not exist a $\varpi \in \mathbb{R}$ such that both conditions 1 and 2:

$$\textbf{Condition 1}: \quad |\arg \overline{G}(\mathrm{j}\varpi)| = 180^\circ \tag{45}$$

$$\textbf{Condition 2}: \quad |\overline{G}(\mathrm{j}\varpi)| > 1, \tag{46}$$

are satisfied, then asymptotic stability is guaranteed.

The conservatism of this reformulation comes from the particular case where the Nyquist contour $\Gamma_{\overline{G}(s)}$ passes $|\arg \overline{G}(\mathrm{j}\varpi)| = 180^\circ$ at $|\overline{G}(\mathrm{j}\varpi)| > 1$ twice without passing $|\arg \overline{G}(\mathrm{j}\varpi)| = 180^\circ$, $|\overline{G}(\mathrm{j}\varpi)| < 1$ in between and consequently not encircling -1.

Recall the two terms $\overline{G}_a(\bar{s}), \overline{G}_t(\bar{s})$ of the characteristic equation, as given in (36), (37). The Bode diagram of these loop transfer functions, for a particular parameter setting, is shown in Fig. 7, while the sum, the loop transfer function $\overline{G}(s)$, is shown in Fig. 9.

As is noted in Section 3.3, K_a is typically quite large, and it has been noted in previous literature that the axial dynamics is unstable for realistic parameter values [18], and dominating with respect to the torsional term with gain $\overline{K}_t$ by a factor of 10^2–10^3 [15]. The axial term being the dominating term in the characteristic equation, the first term $\overline{G}_a$ in $\overline{G} = \overline{G}_a + \overline{G}_t$ should be analyzed when assessing stability, and the torsional term $\overline{G}_t$ can in many cases be considered small in this regard, see Fig. 9. If, however, we would succeed in attenuating the axial term, it may happen that the torsional term becomes significant, in relation to stability properties. In such a case, a full stability analysis using Theorem 1 is needed and additional measures on the torsional

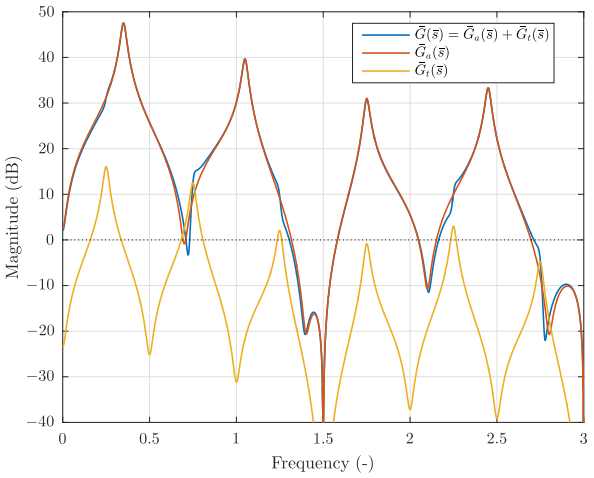

Fig. 9. Bode diagram comparing the magnitudes of the axial and torsional terms, $\overline{G}_a(\bar{s}), \overline{G}_t(\bar{s})$, and their influence on the *total loop transfer function* $\overline{G}(\bar{s})$, here illustrated for a one-section case with $\overline{K}_a = 20, \overline{K}_t = 1, \eta_a = \eta_t = 0.82, \bar{c} = 1.4, \overline{\Omega} = 1.5$.

dynamics may have to be taken as well to guarantee stability.

We note again that considering each of the axial and torsional terms $\overline{G}_a(\bar{s}), \overline{G}_t(\bar{s})$ in isolation is formally not sufficient for determining stability, as this must be evaluated by employing the stability criterion on $\overline{G}(\bar{s})$. But, developing heuristics using $\overline{G}_a(\bar{s}), \overline{G}_t(\bar{s})$ is helpful since it provides physics-based insight as to how the stability properties of the drill string can be associated to the axial and torsional dynamics and to drill-string and bit rock interaction properties. Considering $\overline{G}(\bar{s})$ directly is difficult due to the complexity and richness of the related dynamics. Consequently, we will, in the following Sections 4.2 and 4.3, analyze the axial and torsional feedback loops separately.

4.2. Axial dynamics

For the axial dynamics, we will check the conditions:

$$\textbf{Cond. A1}: \quad |\arg \overline{G}_a(\mathrm{j}\varpi)| = 180°. \tag{47}$$

$$\textbf{Cond. A2}: \quad |\overline{G}_a(\mathrm{j}\varpi)| > 1. \tag{48}$$

Considering condition **A1**, we note from Fig. 5 that we have

$$-90° \leq \arg \overline{g}_a(\mathrm{j}\varpi) \leq 90°, \tag{49}$$

that is, the drill string transfer function is passive. The same can be shown to hold for the delay term. Thus, considering the phase contribution of each of the factors in the axial term $\overline{G}_a(\bar{s}) = \overline{g}_a(\bar{s})\frac{\overline{K}_a}{\bar{s}}\left(1 - e^{-\bar{s}/\overline{\Omega}}\right)$, we have that:

$$\arg \frac{1}{\mathrm{j}\varpi} = -90° \tag{50}$$

$$|\arg \overline{g}_a(\mathrm{j}\varpi)| < 90° \tag{51}$$

$$|\arg(1 - e^{-\mathrm{j}\varpi/\overline{\Omega}})| \leq 90°. \tag{52}$$

Adding up the phase contributions we obtain from **A1**:

$$-90° = \arg(1 - e^{-\mathrm{j}\varpi/\overline{\Omega}}) + \arg g_a(s), \tag{53}$$

and consequently condition **A1** can only be satisfied when the phase contributions of the delay factor and $g_a(s)$ are both negative. For the delay factor this equates to

$$\arg(1 - e^{-\mathrm{j}\varpi/\overline{\Omega}}) < 0°, \tag{54}$$

which occurs (see also Fig. 8) for frequencies satisfying

$$\pi\overline{\Omega}(2n-1) < \varpi < \pi\overline{\Omega}(2n), \quad n = 1, 2 \ldots. \tag{55}$$

which express the frequency ranges where the axial term $\overline{G}_a(\bar{s})$ may cause instabilities, as given by condition **A1**. In this frequency range, the phase of $\overline{G}_a(\bar{s})$ may cross the 180°, at which point condition **A2** must be checked.

Consider again Fig. 7, in the frequency range $\varpi \in [0.75, 1.5]$, indicated in gray, there is the possibility of an axial instability. The phase of $\overline{G}_a(\bar{s})$ crosses the 180° line at the frequency 1.07, at which point we see that the axial magnitude is also above 0 dB, indicating instability cf. condition **A2**. The same conditions for instability are also satisfied at frequency $\varpi = 2.48$, meaning that for the considered parameter set there are multiple unstable axial modes.

It can be difficult to draw general conclusions from the graphical Nyquist criterion. Hence, toward the goal of quantifying the effect of the model parameters on the system stability, conservative stability conditions, explicit in the system parameters, are stated below.

Proposition 1. *Adopt the approximation in (39), for $i = a$. A sufficient stability condition for the characteristic equation $\overline{G}_a(\bar{s}) + 1 = 0$ for the single section drill-string is*:

$$2\frac{1+|\eta_a|}{1-|\eta_a|}\frac{\overline{K}_a}{\overline{\Omega}\pi} < 1, \tag{56}$$

which is equivalent with

$$\frac{1+|\eta_a|}{1-|\eta_a|}\frac{4}{\overline{\omega}}\frac{a\zeta\epsilon}{\zeta_a} < 1. \tag{57}$$

Proof The proof can be found in Appendix D. □

Proposition 2. *Assume that the following bound, derived in (C.12) in Appendix C.2, holds*:

$$|g_i(s)| \le |g_m(s)|\frac{1+|\eta_i|}{1-|\eta_i|} \le \frac{1+|\eta_i^c|}{1-|\eta_i^c|}\frac{1+|\eta_i|}{1-|\eta_i|}, \tag{58}$$

a sufficient stability condition for the characteristic equation $\overline{G}_a(\bar{s}) + 1 = 0$ for the two section drill-string is:

$$\frac{1+|\eta_a|}{1-|\eta_a|}\frac{4}{\overline{\omega}}\frac{a\zeta\epsilon}{\zeta_a^p} < 1. \tag{59}$$

Proof The proof can be found in Appendix D. □

Remark 3. It is worth noting that (57) is independent of the drill string length and the number of cutters on the bit, both of which one would expect to have an influence on the axial stability. This means that, according to this conservative heuristic, axial stability is dependent only on: a relative magnitude between the bit rock interaction and the drill string parameters, the RPM and the amount of damping in the system. For the case of axial impedance matching, $\eta_a = 0$, we have the sufficient condition for axial stability

$$\frac{4}{\overline{\omega}}\frac{a\zeta\epsilon}{\zeta_a} < 1, \tag{60}$$

which still might be hard to achieve in practice, given the typical parameter ranges given in Section 3.2.

Remark 4. Condition (59) is slightly more conservative than (56) due to the fact that worst-case gain, as given by the bound (C.12), occurs much more rarely (in the frequency domain), and not necessarily within the frequency range expressed by (55), as will be discussed in Section 5.2. Note that (57) is equivalent with (59) if ζ_a in the single section drill string is taken to be equal to the pipe impedance ζ_a^p in the two-section case.

4.3. Torsional dynamics

Similar to the analysis of the axial term, we can consider the effect of the torsional term $\overline{G}_t(\bar{s})$. We have the torsional "conditions for instability":

$$\textbf{Cond. B1}: \quad |\arg \overline{G}_t(\mathrm{j}\varpi)| = 180° \tag{61}$$

$$\textbf{Cond. B2}: \quad |\overline{G}_t(\mathrm{j}\varpi)| > 1. \tag{62}$$

Note the difference in sign of the axial term and the torsional term, cf. (36) and (37). This difference is the cause of axial and torsional instability frequency regions indicated in Fig. 7. Furthermore, for typical values of $\overline{K}_t$, we have

$$\left|\left(1-e^{-\bar{s}/\overline{\Omega}}\right)\frac{\overline{K}_t}{\bar{s}}\right| < 1. \tag{63}$$

Recall that $\overline{g}_t(\overline{s})$ varies around 1 with the resonances and anti-resonances whose amplitudes depends on the parameter η_t. Hence, the points where condition **B2** is satisfied tend to be due to resonances in $\overline{g}_t(\overline{s})$, see also Fig. 7.

In particular we note from Fig. 5 that the resonances can be avoided in the one-section case, and, from Fig. 6, significantly reduced in the two section case, by impedance matching, i.e. setting the load impedance $Z_t^L \approx \zeta_t^p$ to obtain $\overline{g}_t(\overline{s}) \approx 1$. Due to the fact that the torsional loop gain, $\overline{K}_t$, tends to be small, applying such impedance matching can remove the torsional instability by ensuring that condition **B2** is never satisfied. The following sufficient condition for stability is derived in Appendix D.

Proposition 3. *Adopt the approximation in (39). A sufficient stability condition for the characteristic equation $\overline{G}_t(\overline{s}) + 1 = 0$ for the single section drill-string is, for $\eta_t > 0$:*

$$4\overline{K}_t \frac{1}{\pi} \frac{1+|\eta_t|}{1-|\eta_t|} < 1. \tag{64}$$

For $\eta_t < 0$, a sufficient stability condition is:

$$2\overline{K}_t \frac{1}{\pi} \frac{1+|\eta_t|}{1-|\eta_t|} < 1. \tag{65}$$

Proof The proof can be found in Appendix D. □

Proposition 4. *Adopt the bound (58). A sufficient stability condition for the characteristic equation $\overline{G}_t(\overline{s}) + 1 = 0$ for the two section drill-string is, for $\eta_t > 0$:*

$$4\overline{K}_t \frac{1}{\pi} \overline{\zeta}_t \frac{1+|\eta_t|}{1-|\eta_t|} < 1. \tag{66}$$

For $\eta_t < 0$ a sufficient condition is:

$$2\overline{K}_t \frac{1}{\pi} \overline{\zeta}_t \frac{1+|\eta_t|}{1-|\eta_t|} < 1. \tag{67}$$

Proof The proof can be found in Appendix D. □

The only difference between (64) and (66) is the appearance of $\overline{\zeta}_t$ (the relative impedance between the pipe and the collar section), which increases the worst-case gain of the two-section drill string. However, K_t also contains ζ_t^c in stead of ζ_t in the two-section case, as noted for the axial case.

Remark 5. We note that from the sufficient condition (64), that there are two apparent ways of stabilizing the torsional loop: increasing damping, o.e. lowering η_t, (to reduce magnitude of the resonance) and lowering the torsional loop gain $\overline{K}_t$. We note that the latter is proportional to ROP and length of the drill string, and inversely proportional to RPM. Further note the conservatism of the bound $\left(1 - e^{-\overline{s}/\overline{\Omega}}\right) \leq 2$ in (D.7), in that the magnitude of this delay term decreases towards zero as $\overline{\Omega}$ is increased (by increasing RPM or the length of the drill-string). This effect comes in addition to the decrease in $\overline{K}_t$ for an increase in RPM, while when increasing the length of the drill-string these two effects will counteract each other.

Remark 6. Using topside impedance matching of the torsional dynamics to avoid resonances, as used above, is the approach used by Shells Z-Torque system [29]. The physical constraints of the actuation, however, limits the frequency range over which effective impedance matching can be achieved. Noting that the loop gain rolls of at higher frequencies due to the integration term, the main concern is addressing the resonances of the first couple of low frequency modes. This observation has also been the key driver behind the work in [8,10,37] on other control strategies for stick-slip mitigation specifically targeting the damping of the lowest resonance modes in the torsional dynamics.

Remark 7. We care to stress that even when the torsional instability could be resolved, e.g. by impedance matching, the axial instability may still perceivably lead to torsional (stick-slip) vibrations. Previous works [18–21,37] have shown that the limit cycle caused by an axial instability (i.e., the non-local axial dynamics) can invoke a velocity-weakening effect in the torque on bit, which, in turn, may cause torsional stick-slip limit cycling, even when the isolated torsional dynamics is localy asymptotically stable. Therefore, it is interesting to study measures to also target the axial instability, and use the linear stability analysis as a starting point to analyze the rather complex non-linear distributed dynamics, also in a non-local sense. For now the results in Section 5 will focus on addressing the local stability properties of the system in the parametric space introduced in Section 3.

Remark 8. For the RGD model the conditions **B1** and **B2** can be used to derive the well known criteria from Eqs. (34) and (44) in [35] (see Appendix D.1 for details):

$$\overline{\Omega} < \sqrt{\frac{8\zeta\epsilon a}{NM}}, \tag{68}$$

The right-hand side of (68), however, can be compared with (57), (noting that (57) is a conservative condition):

$$\overline{\Omega} < \frac{1+|\eta_a|}{1-|\eta_a|} \frac{4\zeta\epsilon a}{A^c \rho c_a}. \tag{69}$$

The difference between (68) and (69) is due to a combination of the approximation inherent in the lumped model of (68), and the conservatism in (69). Key differences to note are the appearance of N and resonance magnitude term, respectively.

5. Stability maps

In the preceding section, we argued for analyzing the axial and torsional loop transfer function in isolation in pursuit of a less complex interpretation of the stability result. We also showed that the axial and torsional loop transfer functions, $\overline{G}_a(\bar{s}), \overline{G}_t(\bar{s})$, are specified by the five non-dimensional parameters: $\overline{\Omega}, \overline{K}_i, \eta_i$, for $i \in \{a, t\}$, in the single-section case (assuming $\overline{c} = 1.6$ fixed), with the additional three $\overline{t}_p, \overline{Z}_i^c$ for $i \in [a, t]$, for the two-section case. Finally, we have argued that analyzing the axial and torsional loop transfer functions $\overline{G}_a(\bar{s}), \overline{G}_t(\bar{s})$ in isolation yields insight into the overall behavior of $\overline{G}(\bar{s})$.

When using the Nyquist stability criterion, the robustness of the stability of a system, can be gaged by its *gain margin* [38]. We will in the following refer to the inverse of the gain margin where a positive decibel value of the *inverse gain margin* (indicating an inverse gain margin larger than 1) indicates instability. Since the inverse gain margin is proportional to the nominal loop gain coefficient $\overline{K}_a$, and given the fact that we would like to use a minimal set of parameters to parametrize the stability of the system, we define a normalized inverse gain margin, $M_{G,i}$, $i \in \{a, t\}$, as

$$M_{G,i} \equiv \max_{\varpi \in \varpi_{180}} \left| \frac{\overline{G}_i(\mathrm{j}\varpi)}{\overline{K}_i} \right|, \quad \text{with} \quad \varpi_{180} = \{\varpi \in \mathbb{R} : \angle \overline{G}_i(\mathrm{j}\varpi) = 180^\circ\}. \tag{70}$$

This means that $\overline{K}_i M_{G,i} > 1$ (i.e. exceeds 0 dB) indicates instability, with the severity of the instability given by this product $\overline{K}_i M_{G,i}$. Conversely, $\overline{K}_i M_{G,i} < 1$ means that the system is stable with the robustness of the system given by the same product.

5.1. Single section drill string

For the single section drill string, the stability of the axial and the torsional loop, is respectively determined by the three parameters $\overline{\Omega}, \overline{K}_i, \eta_i$, for $i \in \{a, t\}$. We recall the physical interpretation of these parameters as discussed in Section 3.2:

- $\overline{K}_i$, $i \in \{a, t\}$, is determined dy bit-rock interaction and drill-string parameters. $\overline{K}_t$ additionally includes the RPM to ROP ratio.
- η_i, $i \in \{a, t\}$: related to boundary condition, where small $|\eta_i|$ means that there is a large amount of damping in the system. $\eta_i > 0$ denotes a stiff top-drive where speed is kept relatively constant, while $\eta_i < 0$ denotes a softer top-drive where the torque applied on the drill string is mostly constant.
- $\overline{\Omega}$: RPM relative to drill string length.

5.1.1. Stability analysis for the axial dynamics

For the axial loop, stability is determined by the three parameters $\overline{\Omega}, \overline{K}_a, \eta_a$. That is, specifying a value for $\overline{K}_a$ a two-dimensional stability map can be made parametrized in $\overline{\Omega}, \eta_a$. This is done for the case of $\overline{K}_a = 20$ in Fig. 10. In this figure, the frequency response functions, on which the Nyquist criterion has been applied, are also shown for two specific parameter sets corresponding to a stable and an unstable axial loop. For the frequency response function drawn from the stable parameter set the magnitude, it can be verified that the magnitude is below 0 dB at the frequencies when the phase crosses 180°, and above 0 dB for the unstable set of parameters.

The line giving the boundary between the stable and unstable regions in Fig. 10 is given by

$$M_{G,a} \overline{K}_a = 1. \tag{71}$$

We see in Fig. 10 (and also in Fig. 11, to be introduced) an decrease in $M_{G,a}$ with increases in $\overline{\Omega}$ (faster drill bit rotation rates). This is caused by the fact that a smaller delay, $\overline{t}_N = 1/\overline{\Omega}$, increases the frequency at which the delay factor $1 - e^{-\bar{s}/\overline{\Omega}}$ has a negative phase contribution, which is required for axial instability, cf. **Cond. A1** in Section 4.2. The magnitude of the characteristic equation decays at higher frequencies due to the integrator factor (the s in the denominator, see (36)). These two main trends are consistent with the sufficient condition of Proposition 1.

Fig. 10 shows clearly so-called stability lobes characteristic to delay systems and also shows that high RPM $\overline{\Omega}$ and low reflection coefficient η_a are beneficial for stability.

Given (71) as the stability boundary, since $\overline{K}_a$ is a scaling of the axial term of the characteristic equation, $\overline{G}_a(\bar{s})$, plotting the normalized inverse gain margin, $M_{G,a}$, parametrized in $\overline{\Omega}$ and η_a gives a complete parametrization of the stability of the axial loop of the single section drill string. This is shown in Fig. 11.

Fig. 11, shows that the damping in the system, corresponding to a small pseudo reflection coefficient η_a, is beneficial for stability. For the axial term, typical values of $\overline{K}_a \sim 40 - 60$ dB, imply that, in order to guarantee that $M_{G,a} K_a < 1$, almost perfect impedance matching would be required to avoid instability: i.e. $\eta_a \approx 0$.

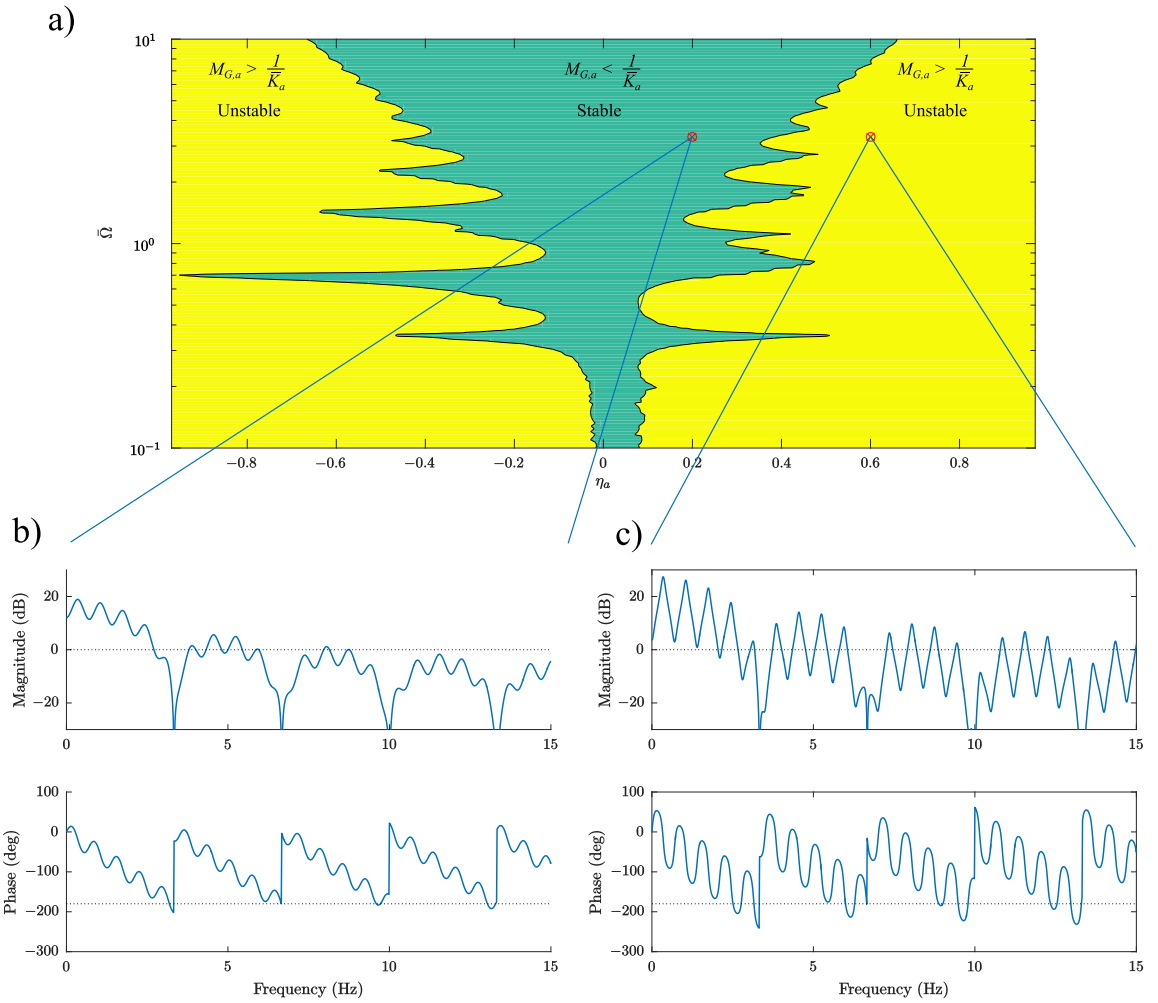

Fig. 10. a) Axial stability map for $\overline{K}_a = 20$ (i.e., 26 dB) parametrized in the dimensionless angular velocity $\overline{\Omega}$ and pseudo reflection coefficient η_a, for the single section drill string. Example frequency response functions are also shown for b) $\overline{\Omega} = 3.33, \eta_a = 0.2$ and c) $\overline{\Omega} = 3.33, \eta_a = 0.6$.

5.1.2. Stability analysis for the torsional dynamics

For the torsional loop, the stability is determined by the three parameters $\overline{\Omega}, \overline{K}_t, \eta_t$. Again, specifying a value for $\overline{K}_t$ a two-dimensional stability map can be made parametrized in $\overline{\Omega}, \eta_t$. This is done for the case of $\overline{K}_t = 1$ in Fig. 12.

Plotting the normalized inverse gain margin, $M_{G,t}$, parametrized in $\overline{\Omega}$ and η_t gives a complete parametrization of the stability of the axial loop of the single section drill string. This is shown in Fig. 13. Again, in Figs. 12 and 13, we note that the damping in the system, corresponding to a small pseudo reflection coefficient η_i, $i \in \{a, t\}$, is beneficial for stability. In the region $\overline{\Omega} > 1$, increasing $\overline{\Omega}$ also has an almost uniformly stabilizing effect (see Fig. 14).

A noticeable difference from the axial stability map is the absence of the lobes in the region $\eta_t > 0$, $\overline{\Omega} > 1$, which is due to the first resonance mode of $\overline{g}_t$ being located in the frequency range where the delay term has a positive phase contribution, required for **Cond. B1**, and consequently this is consistently the dominating unstable mode. This is different from the axial term in the $\eta_t > 0$, $\overline{\Omega} > 1$ region, where the *most* unstable mode changes as the angular velocity is increased, see Fig. 11. Note that increasing the angular velocity $\overline{\omega}$, in addition to increasing $\overline{\Omega}$, also decreases the torsional nominal loop gain $\overline{K}_t$, both of which contributes to stability. Comparing with the sufficient condition of Proposition 3, we observe that $\overline{\Omega}$ does not appear in (64), meaning that the effect of increasing $\overline{\Omega}$ is not captured, and that this specific sufficient condition can entail a significant conservatism.

Finally, to enable easier comparison with stability analysis on lumped-parameter models that have been performed in the literature, stability maps parametrized in imposed axial and angular velocities is given in Fig. 15.

From Fig. 15, the following observations can be made:

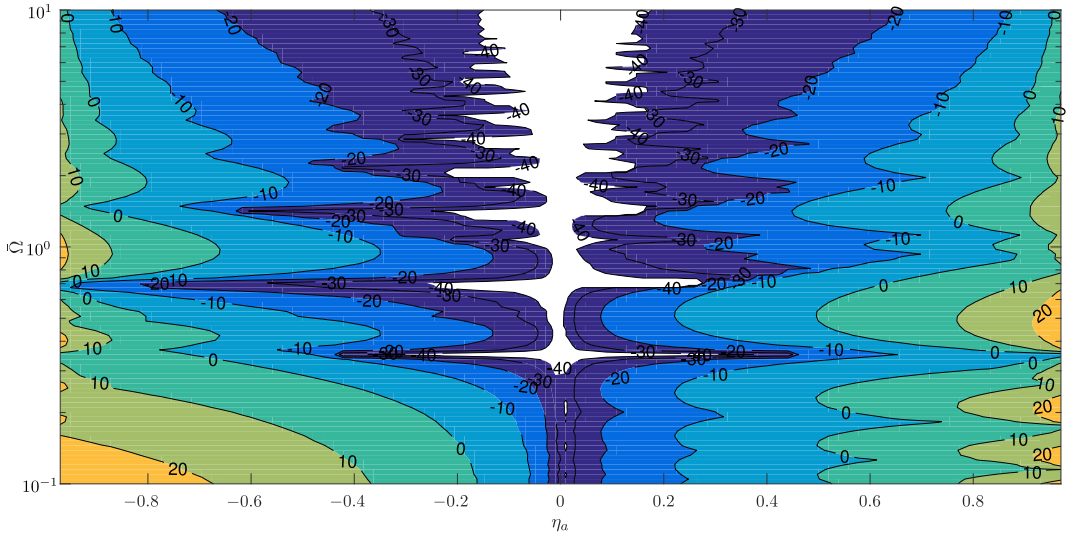

Fig. 11. Axial loop normalized inverse gain margin in dB, $M_{G,a} = \max_{\varpi \in \varpi_{180}} \left| \frac{\overline{c}_a(j\varpi)}{K_a} \right|$, parametrized in the dimensionless angular velocity, $\overline{\Omega}$, and pseudo reflection coefficient η_a, for the single section drill string.

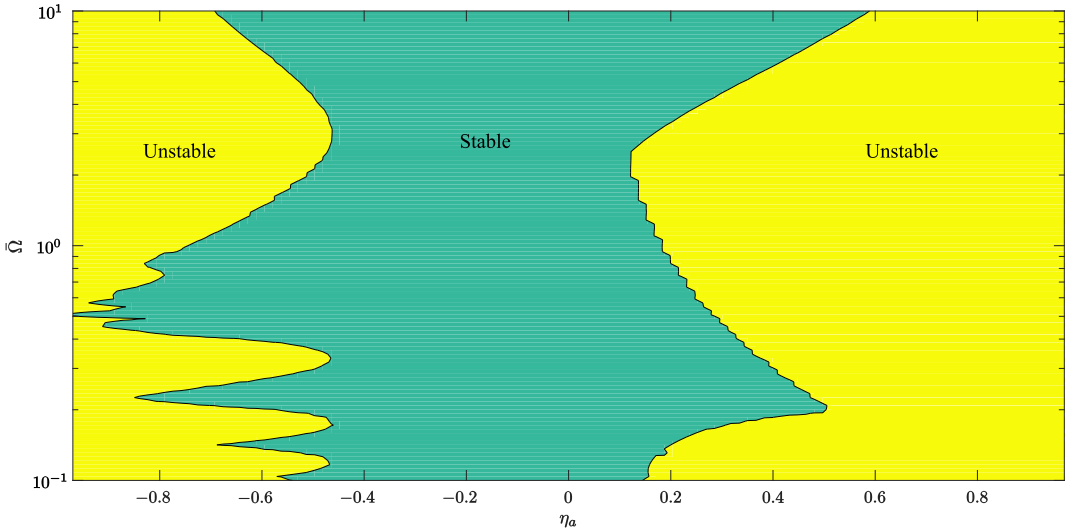

Fig. 12. Torsional stability map for $\overline{K}_t = 1$ (i.e. 0 dB) parametrized in the dimensionless angular velocity $\overline{\Omega}$ and pseudo reflection coefficient η_t, for the single section drill string.

- $\eta_a < 0$ (i.e. a soft top-drive) leads to larger stability areas than $\eta_t > 0$ (i.e. a stiff top-drive);
- A low reflection coefficient enlarge the stability area;
- Increasing RPM, $\overline{\Omega}$ is beneficial for stability;
- High ROP is disadvantageous for stability.

5.2. Two-section drill string

We now turn to the case of a drill string with two sections. For this case we need the additional three parameters $\overline{t}_p$ and $\overline{Z}_i^c$, for $i \in [a, t]$, to fully describe the characteristic function. Here we recall from Section 3.2.2 that $\overline{t}_p \in [0, 1]$ gives travel time of the lower drill-string section relative to the travel time of the full drill string (effectively giving the relative length of the lower section) and $\overline{Z}_i^c$ denotes the impedance of the lower section relative to the impedance of the upper section.

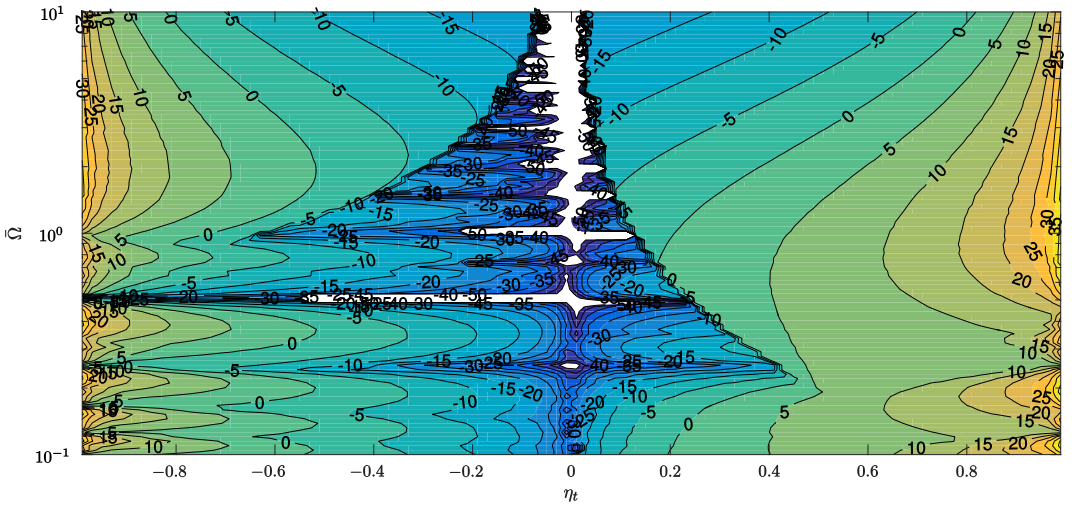

Fig. 13. Torsional loop normalized inverse gain margin, $M_{G,t} = \max_{\varpi \in \varpi_{180}} \left| \frac{\overline{G}_t(j\varpi)}{K_t} \right|$, parametrized in the dimensionless angular velocity $\overline{\Omega}$ and pseudo reflection coefficient η_t, for the single section drill string. Note that the increasing the angular velocity $\overline{\omega}$, in addition to increasing $\overline{\Omega}$, also decreases the torsional nominal loop gain $\overline{K}_t$.

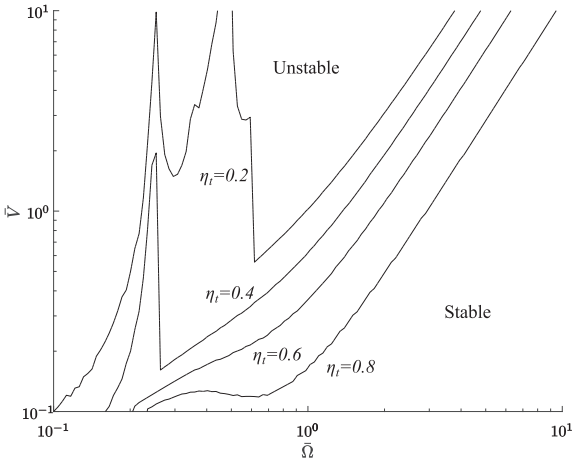

Fig. 14. Torsional stability boundaries parametrized in non-dimensional angular, $\overline{\Omega}$, and axial, $\overline{V} = \bar{v}\frac{N^2 \bar{t}_t^2 a^2 \epsilon}{\zeta_t 4\pi} = \overline{\Omega K}_t$, velocities for positive pseudo reflection coefficients η_t.

5.2.1. *Stability analysis of the axial dynamics*

Initially we consider a comparison with the single section case by specifying the parameters $\overline{K}_a = 20, \bar{t}_p = 0.9, \overline{\zeta}_a = 3$, and plotting the two-dimensional stability map parametrized in $\overline{\Omega}, \eta_a$. This is shown in Fig. 16.

By comparing Figs. 10 and 16 we observe that for the considered, typical, values for the lower drill-string section the stable region is significantly decreased for low RPMs $\overline{\Omega}$.

To obtain a complete a more complete visualization of the effect of all the five parameters on the stability, we fix η_a, and instead use $\bar{t}_p$ along the horizontal-axis. The normalized inverse gain margin, $M_{G,a}$, for a two-section drill-string parametrized in $\bar{t}_p$ and $\overline{\zeta}_a$ for the axial loop transfer function is shown in Figs. 17 and 18. The four figures correspond to high (left, $\eta_a = \pm 0.5$) and low (right, $\eta_a = \pm 0.8$) damping and small (top, $\overline{\zeta}_a = 3$) and large (bottom, $\overline{\zeta}_a = 9$) relative impedance between the pipe and collar sections.

As for the single section case, the damping, as represented by the reflection coefficient η_a is important. A smaller $|\eta_a|$ tends to decrease $M_{G,a}$ uniformly, while retaining the shape of the parametrized stability map. The $\overline{\zeta}_a$ parameter indicates how important the collar section is to the overall dynamics, where $\overline{\zeta}_a = 1$ reduces the system to the single section case. A large $\overline{\zeta}_a$ exaggerates the features of the map, increasing the prominence of peaks and troughs. Consequently, the addition of drill collars to the drill string can increase or decrease the inverse gain margin, compared to the single section case, depending on the specific operating

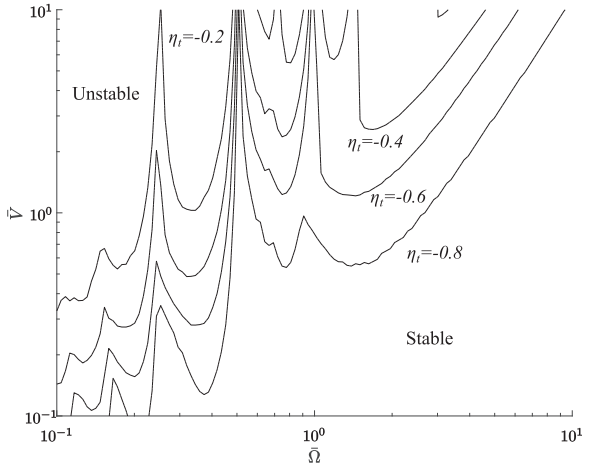

Fig. 15. Torsional stability boundaries parametrized in non-dimensional angular, $\overline{\Omega}$, and axial, $\overline{V} = \overline{v}\frac{N^2 t_c^2 a^2 \epsilon}{\zeta_t 4\pi} = \overline{\Omega K}_t$, velocities for negative pseudo reflection coefficients η_t.

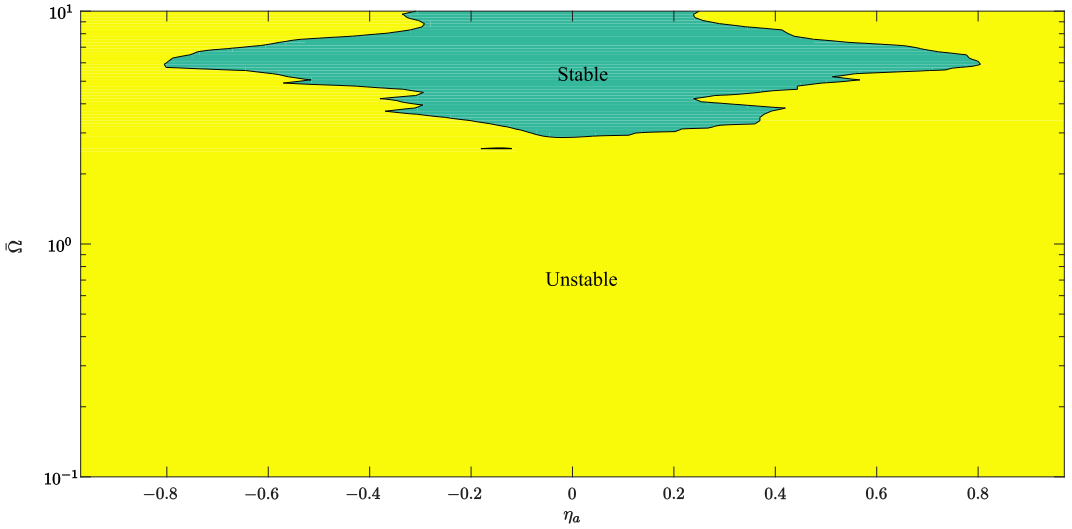

Fig. 16. Axial stability map for two section drill-string with parameters $\overline{K}_a = 20, \overline{t}_p = 0.9, \overline{\zeta}_a = 3$ parametrized in the dimensionless angular velocity $\overline{\Omega}$ and pseudo reflection coefficient η_a, cf. Fig. 11.

parameters.

As a general trend, observe again that, as for the single section drill string, the inverse gain margin becomes smaller for larger RPM ($\overline{\Omega}$). Furthermore, a prominent feature of Fig. 17 is a valley of significantly reduced values of $M_{G,a}$ compared to the neighboring regions. This feature can is made more explicit in Fig. 19 which shows the stability of axial loop parametrized with the parameters $\overline{K}_a = 20, \eta_p = 0.5, \overline{\zeta}_a = 3$ fixed. We find this to be due to the anti-resonance of the collar section, which effectively creates a lower loop gain in a frequency area (cf. Fig. 6), coinciding with the area of negative phase contribution of the delay term (necessary for instability cf. **Cond. A1** in Section 4.2). This effect is illustrated in Fig. 20, where axial frequency response functions corresponding to angular velocities above, in and below the valley is shown. Note how the gain of $\overline{G}_a(\overline{s})$ tends to be suppressed when the phase crosses $-180°$ for the middle Bode diagram. Observe that the resonance frequencies of the collar section are given by

$$\varpi_r = \frac{\pi n_r}{\overline{t}_c}, \quad n_r = 0, 1, 2 \ldots, \tag{72}$$

while the areas with positive phase contribution of the delay term correspond to

$$\overline{\Omega}\pi(2n_p) < \varpi < \overline{\Omega}\pi(2n_p + 1), \quad n_p = 0, 1, 2 \ldots. \tag{73}$$

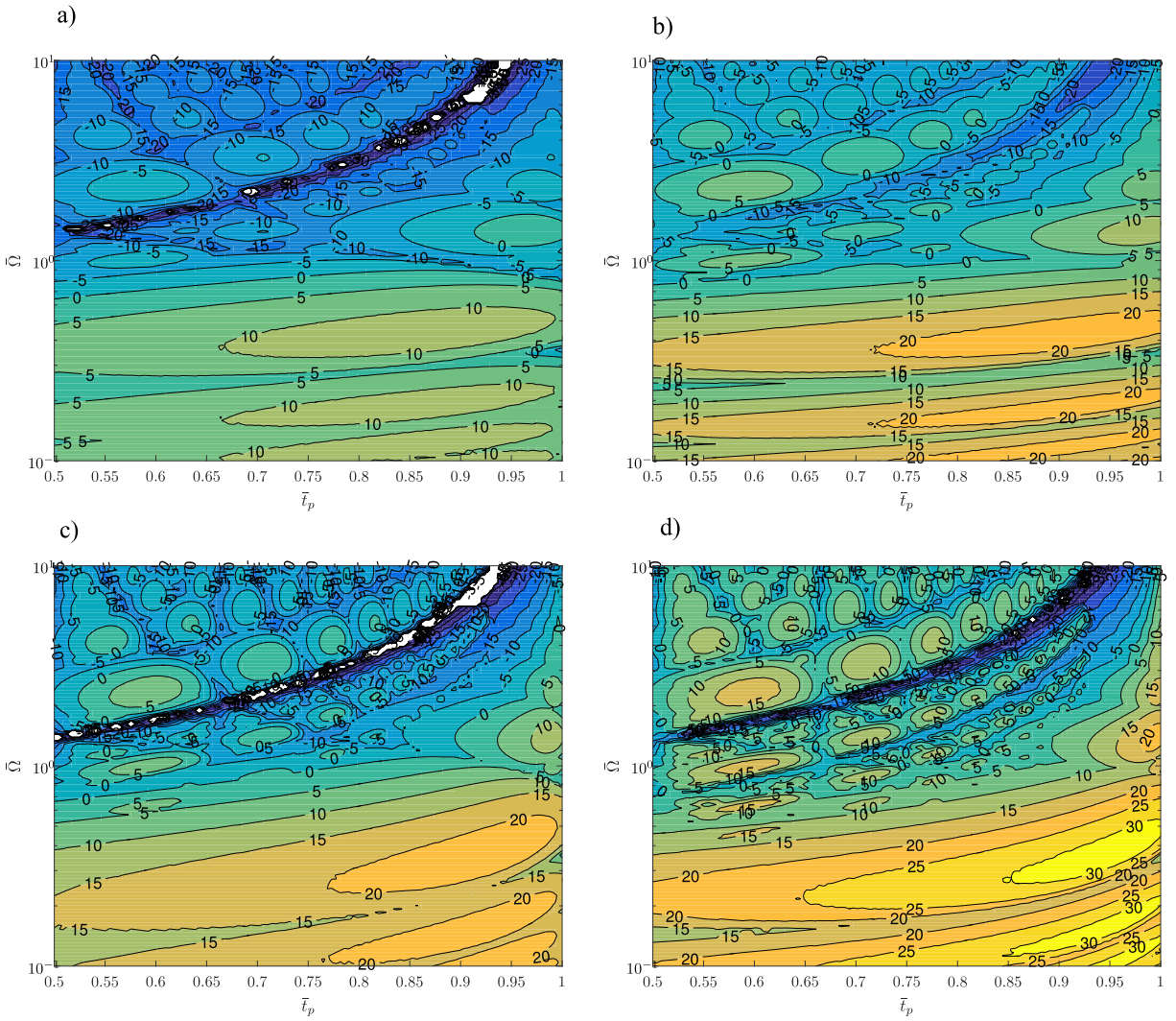

Fig. 17. Axial loop transfer function normalized inverse gain margin, $M_{C,a}$ in dB, maps for two section pipe with a positive pseudo reflection coefficient and parameter sets: a) $\overline{\zeta}_a = 3,\ \eta_a = 0.5$, b) $\overline{\zeta}_a = 3,\ \eta_a = 0.8$, c) $\overline{\zeta}_a = 9,\ \eta_a = 0.5$, d) $\overline{\zeta}_a = 9,\ \eta_a = 0.8$.

The most prominent valley in the inverse gain margin is obtained for $n_p = n_r$; in this case, we have:

$$\pi\overline{\Omega}(2n_p) < \varpi_r < \pi\overline{\Omega}(2n_p + 1) \tag{74}$$

$$\Rightarrow\ 2\bar{t}_c < \frac{1}{\overline{\Omega}} < 2\bar{t}_c + \frac{1}{n_r}\bar{t}_c. \tag{75}$$

This is a quite coarse simplification as, perhaps the most important part of the dynamics, the resonance modes of the full drill string are not directly accounted for. However, a lower inverse gain margin seems to be achieved just above $\overline{\Omega}2\bar{t}_c = 2$, that is, the region where (75) is satisfied for $n_r > 1$. The range $\frac{1}{\overline{\Omega}} \in [2\bar{t}_c, 2.5\bar{t}_c]$ (where $n_r = 2$ has been taken for purpose of illustration of the region), is indicated by red lines in Fig. 20, which indicates the value of the above approximative analysis.

5.2.2. Stability analysis of the torsional dynamics

Again, we consider a comparison with the single section case by specifying the parameters $\overline{K}_t = 1, \bar{t}_p = 0.9, \overline{\zeta}_t = 3$, and plotting the two-dimensional stability map parametrized in $\overline{\Omega}, \eta_a$. This is shown in Fig. 21. By comparing Figs. 12 and 21 we observe that for the torsional loop, and the considered case of typical values, the lower drill-string section does not have a very large effect on stability.

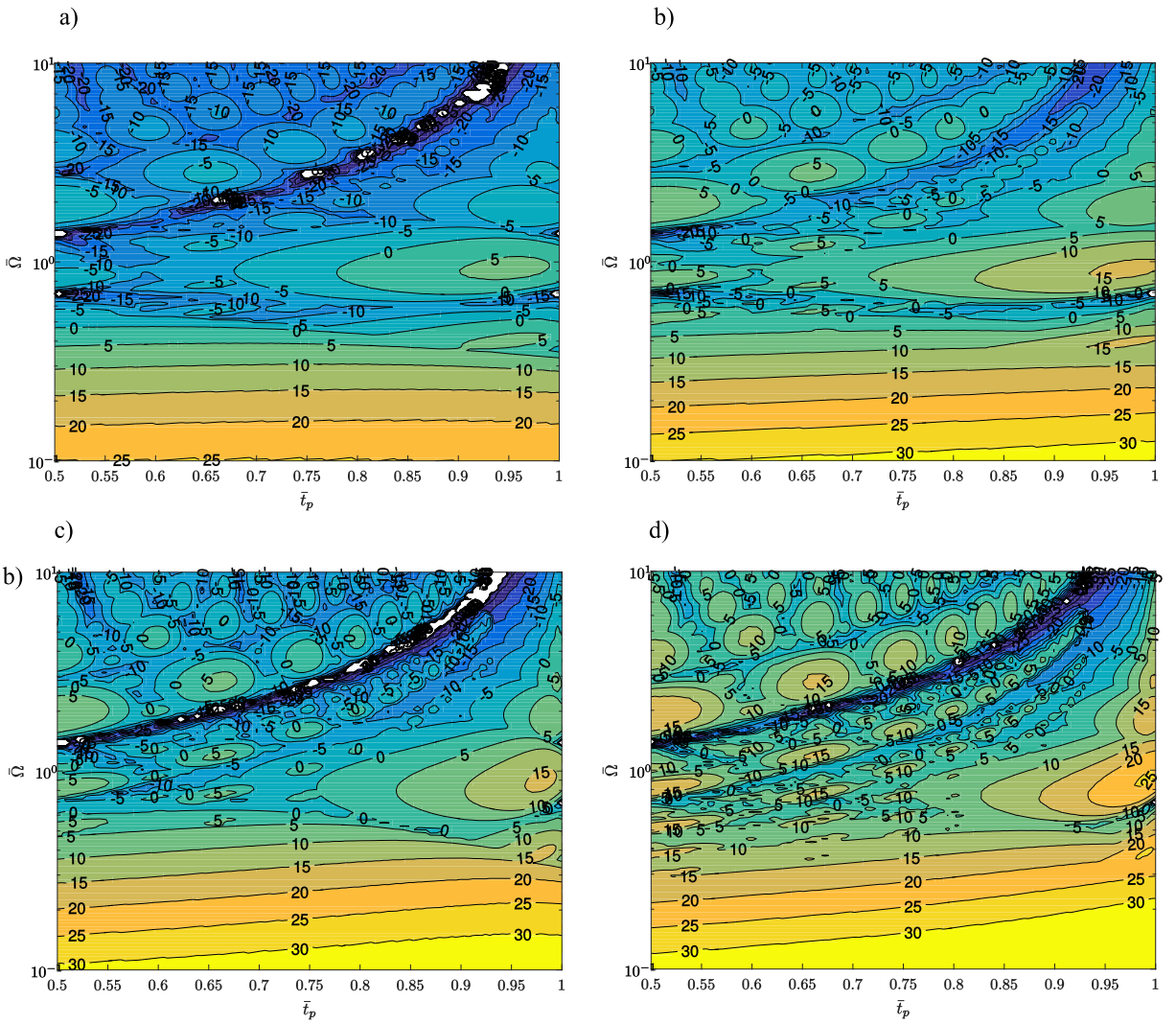

Fig. 18. Axial loop transfer function normalized inverse gain margin, $M_{G,a}$ in dB, maps for two section pipe with a negative pseudo reflection coefficient and parameter sets: a) $\overline{\zeta}_a = 3,\ \eta_a = -0.5$, b) $\overline{\zeta}_a = 3,\ \eta_a = -0.8$, c) $\overline{\zeta}_a = 9,\ \eta_a = -0.5$, d) $\overline{\zeta}_a = 9,\ \eta_a = -0.8$.

For a more complete visualization, we again fix η_t, and instead use $\overline{t}_p$ along the horizontal-axis and plot the normalized inverse gain margin, $M_{G,t}$, for a two-section drill-string parametrized in $\overline{t}_p$ and $\overline{\zeta}_t$ for the torsional loop transfer function. This is shown in Figs. 22 and 23. The four figures correspond to high (left, $\eta_t = \pm 0.5$) and low (right, $\eta_t = \pm 0.8$) damping and small (top, $\overline{\zeta}_t = 3$) and large (bottom, $\overline{\zeta}_t = 9$) relative impedance between the pipe and collar sections.

Due to the first resonance mode being the dominating unstable mode in most instances for the torsional loop, the shape of the features of the map is significantly simpler than for the axial term. Note that typical drilling parameters are $\Omega \in [0.4, 4]$ and $\overline{t}_p \in [0.7, 0.95]$. In this range, the maps indicate that *instability* is associated with

1. Increasing $\overline{t}_p$ – shorter collar section.
2. Increasing $\overline{\eta}_t$ – A high reflection at the top-drive and little damping in the domain. Also note that negative $\overline{\eta}_t$ tends to be preferable to positive.
3. Increasing $\overline{\zeta}_t$ – Increasing the polar moment of inertia of the drill collar section relative to that of the drill pipes.
4. *Decreasing* $\overline{\Omega}$ – lower RPM.

For the combination of low $|\overline{\eta}_t|$ (in particular for $\overline{\eta}_t < 0$), $\overline{\Omega}$ and $\overline{t}_p$ a region of significantly reduced inverse gain margin appears which occurs when **Cond. B1**, in Section 4.3, is not satisfied in the first region of positive phase contribution by the

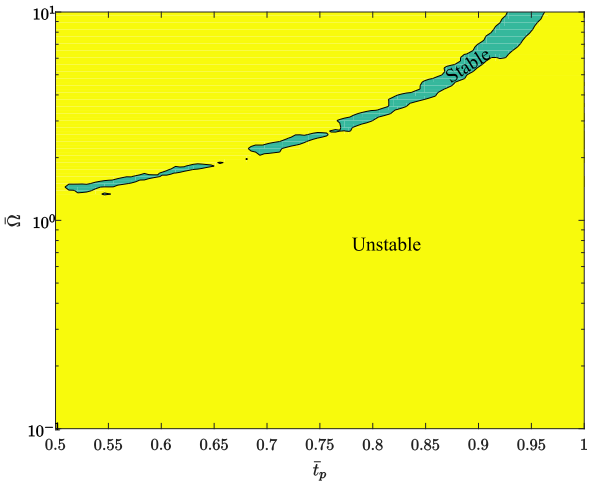

Fig. 19. Axial stability map for two section drill-string with parameters $\overline{K}_a = 20, \eta_p = 0.5, \overline{\zeta}_a = 3$.

delay term. As points 1 and 3 are related to drill string geometry, reducing th tendency to torsional instability is best addressed through point 2 (i.e. reducing the reflection coefficient through attempting impedance matching) and 4. Point 2 and 3 are also represented in (66), while point 1 and 4 are not captured by this sufficient condition. These effects are the result of more complex interactions of phase and gain contributions of the torsional factors and not easily captured by a simple heuristic such as Proposition 4. This illustrates the merit of pursuing the detailed stability maps in this section.

5.3. Discussion of the stability maps

As we have seen in this section, the stability maps for the drill string system are complex, and the effect of varying one parameter is seldom uniform in the other parameters, in particular for the case of a two-section drill string. The main trend that we have identified, however, is that increasing RPM and decreasing the reflection coefficient tend to decreases the inverse gain margin, thereby increasing the tendency for stability, for typical parameter values.

For the torsional case, negative reflection coefficient, η_t, tend to be preferable to a positive one, when reflections of the same magnitude are compared. We iterate the fact that the high gain of the axial loop coefficient, $\overline{K}_a$, can make avoiding the axial instability infeasible.

6. Exemplary case study

In this section, we illustrate some of the results of the paper by considering an example well with realistic parameters.

6.1. Case description and derivation of characteristic quantities

We consider a well being drilled with a two-section drill string with pipe properties given by length $L^p = 1000$ m, cross sectional area $A^p = 0.0035$ m^2 and polar moment of inertia $J^p = 1.2\text{e-}5$ m^4, and collar properties given by length $L^c = 200$ m, cross sectional area $A^c = 0.015$ m^2 and polar moment of inertia $J^c = 5.2\text{e-}5$ m^4. We assume that both pipe and collars are made of steel with modulus': $E = 200e9$ Pascal, $G = 77e9$ Pascal, and density $\rho = 8000$ kg/m^3. This means we have the following impedances

$$\zeta_a^p = \frac{A^p E^p}{c_a} \approx 140\ 270\ [\text{kg/s}], \quad \zeta_t^p = \frac{J^p G^p}{c_t} \approx 302\ [\text{m}^2\text{kg/s}], \tag{76}$$

$$\zeta_a^c = \frac{A^c E^c}{c_a} \approx 626870\ [\text{kg/s}], \quad \zeta_t^c = \frac{J^c G^c}{c_t} \approx 1\ 288\ [\text{m}^2\text{kg/s}]. \tag{77}$$

Finally, we assume the viscous damping coefficients are given by $k_a = k_t = 0.4$, and constant imposed axial and angular velocities such that the load impedances are infinite $Z_a^L = Z_t^L = \infty$. From these physical parameters, we find the characteristic time $t_* = t_t \approx 0.38$ s.

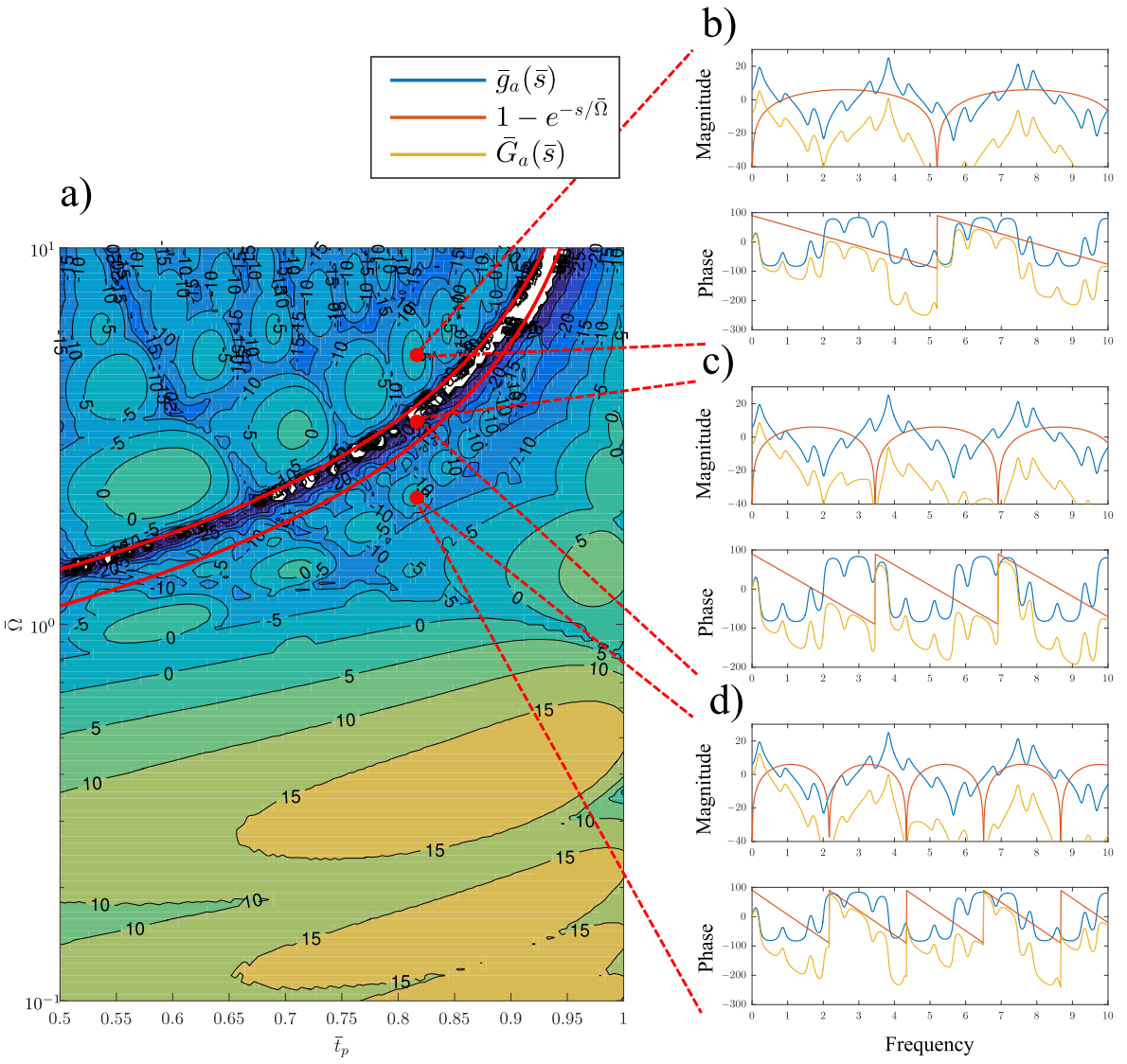

Fig. 20. a) Inverse gain margin map of $M_{G,a}$ showing the computed valley $\frac{1}{\bar{\Omega}} \in [2\bar{t}_c, 2.5\bar{t}_c]$. Bode plots of $\bar{G}_a(\bar{s})$ inside and outside the valley for parameter sets b) $\bar{\zeta}_a = 6,\ \eta_a = 0.5,\ \bar{t}_p = 0.82,\ \bar{\Omega} = 5.20$, c) $\bar{\zeta}_a = 6,\ \eta_a = 0.5,\ \bar{t}_p = 0.82,\ \bar{\Omega} = 3.46$, d) $\bar{\zeta}_a = 6,\ \eta_a = 0.5,\ \bar{t}_p = 0.82,\ \bar{\Omega} = 2.17$.

Now, we derive the corresponding non-dimensional quantities characterizing the drill-string:

$$\bar{c} = \frac{c_a}{c_t} = \sqrt{\frac{E}{G}} \approx 1.61, \tag{78}$$

$$\eta_a = -k_a^d k_a^L = -e^{-2k_a t_a} \frac{\zeta_a^p - Z_a^L}{\zeta_a^p + Z_a^L} \approx 0.83 \tag{79}$$

$$\eta_t = -k_t^d k_t^L = -e^{-2k_t t_t} \frac{\zeta_t^p - Z_t^L}{\zeta_t^p + Z_t^L} \approx 0.73 \tag{80}$$

$$\bar{\zeta}_a = \frac{A^C}{A^p} \approx 4.47 \tag{81}$$

$$\bar{\zeta}_t = \frac{J^c}{J^p} \approx 4.26 \tag{82}$$

$$\bar{t}_p = \frac{L_p}{L_p + L_c} \approx 0.83. \tag{83}$$

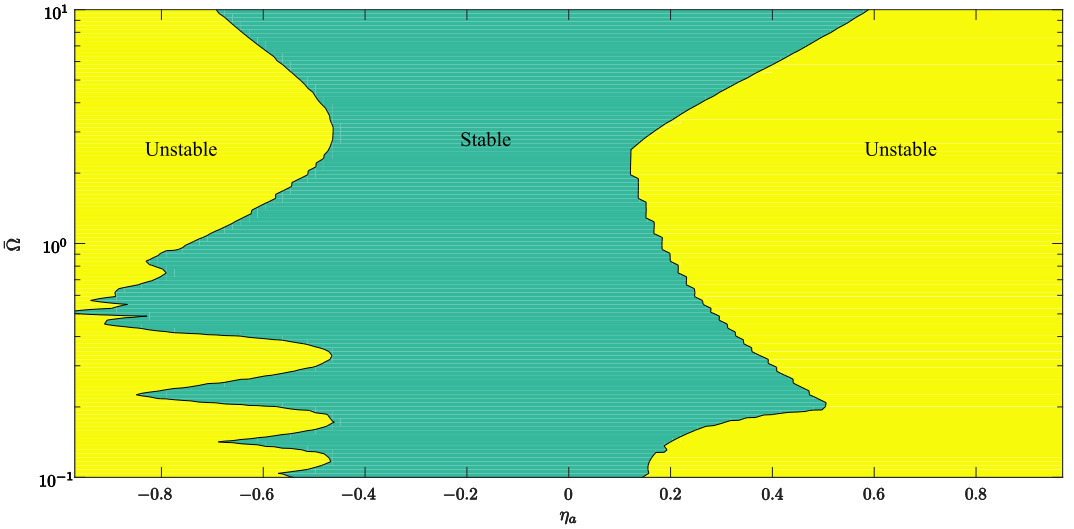

Fig. 21. Torsional stability map for two section drill-string with parameters $\overline{K}_t = 1, \overline{t}_p = 0.9, \overline{\zeta}_a = 3$ parametrized in the dimensionless angular velocity $\overline{\Omega}$ and pseudo reflection coefficient η_t, for the single section drill string.

Next, we consider the following bit-rock interaction parameters: $a = 0.0762$ m, $\zeta = 0.6$, $\epsilon = 60e6$ Pascal and $N = 4$, and, the operational parameters: axial velocity $\overline{v} = 20$ meter/hour, $\overline{\omega}_0 = 90$ RPM. This yields the non-dimensional nominal loop gains as follows:

$$\overline{K}_a = t_* \frac{a\zeta\epsilon N}{\zeta_a} = 6.77, \tag{84}$$

$$\overline{K}_t = t_* \frac{\overline{v}}{\overline{\omega}} \frac{a^2\epsilon N}{2\zeta_t} = 0.12, \tag{85}$$

while the non-dimensional angular velocity is given by

$$\overline{\Omega} = \frac{t_* N}{2\pi}\overline{\omega} = 2.32. \tag{86}$$

6.2. Qualitative analysis using the stability maps

Now, to obtain an impression of the stability of the axial loop, consider the stability map of Fig. 17. We have the axial characteristic quantities $\eta_a = 0.83, \overline{\zeta}_a = 4.47$, so consider subplot **b)** as the closest case. In this subplot we consider the point $\overline{t}_p = 0.83$, $\overline{\Omega} = 2.32$, where we find the axial loop to have a normalized inverse gain margin $M_{G,a} \approx -5$ dB, while nominal axial loop gain is $\overline{K}_a = 16.6$ dB, and hence we expect an axial instability of about 10 dB severity. We also note from the stability map that, in this case, we expect a stabilizing effect from increasing the RPM up until about $\overline{\Omega} = 3.5$.

For the torsional loop we consider the stability map of Fig. 22. We have the torsional characteristic quantities $\eta_t = 0.73, \zeta_t = 4.26$, and hence again consider subplot **b)** as the closest case and the point $\overline{t}_p = 0.83$, $\overline{\Omega} = 2.32$. Here we find the torsional loop to have a normalized inverse gain margin $M_{G,t} \approx 15$ dB (we would expect the actual $M_{G,t}$ to be slightly lower due to the pseudo reflection coefficient $\eta_t = 0.73$ being slightly lower than the $\eta_t = 0.80$ of the stability map). The nominal torsional loop gain is $\overline{K}_t = -18.2$ dB, and hence we do not expect any instability to be caused by the torsional loop.

6.3. Quantitative analysis

We now check these qualitative conclusions against a quantitative stability result. We derive the axial and torsional drill string transfer functions $\overline{g}_i(\overline{s})$, $i \in \{a, t\}$, by using (13). Since $Z_a^L = Z_t^L = \infty$, the relations simplify slightly to

$$\overline{g}_i^p(\overline{s}) = \frac{1}{\sqrt{1 + \frac{k_i}{\overline{s}t_*}}} \tanh\left(\overline{s}t_p \sqrt{1 + \frac{k_i}{\overline{s}t_*}}\right), \tag{87}$$

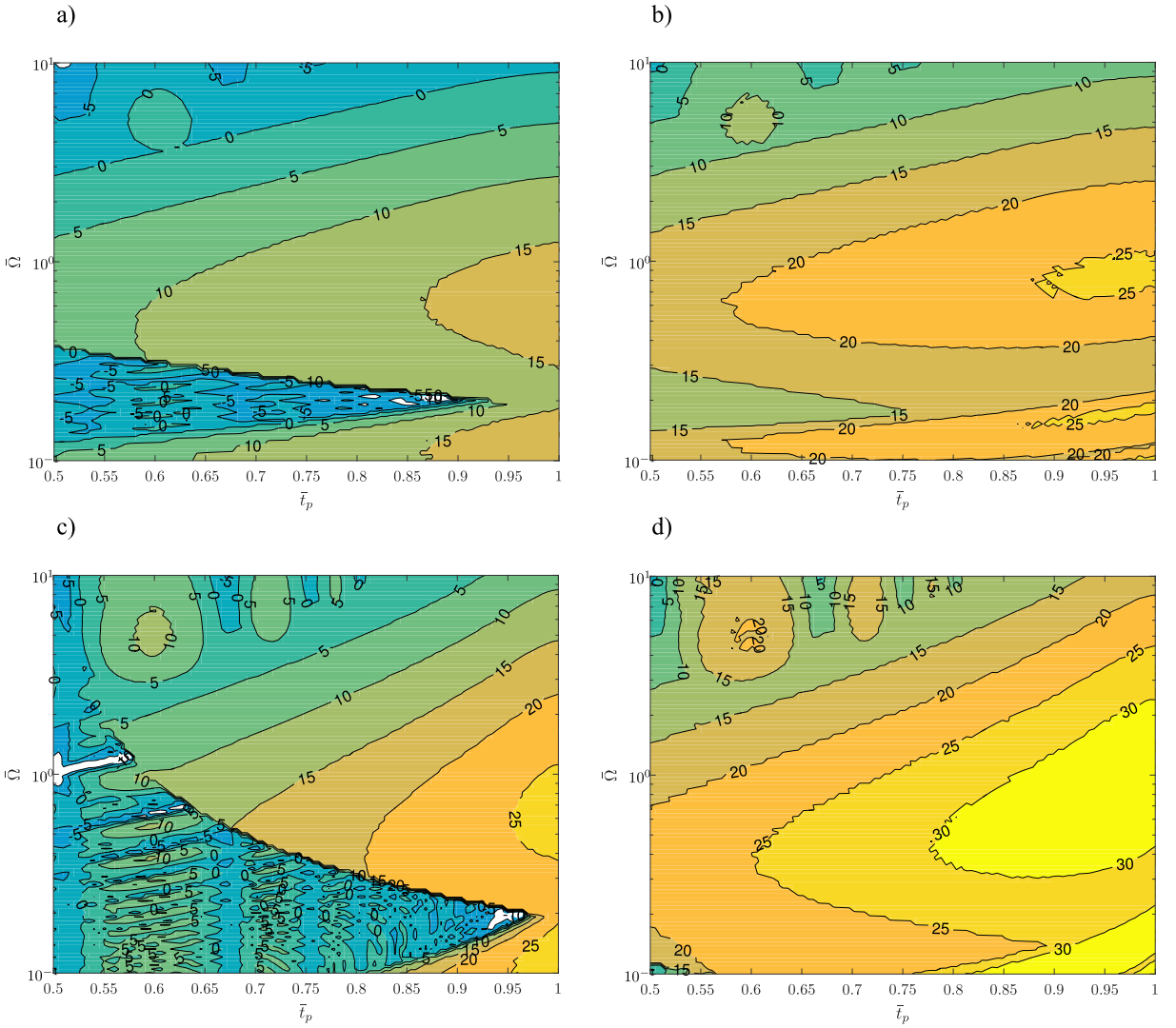

Fig. 22. Torsional loop transfer function normalized inverse gain margin, $M_{G,t}$ in dB, maps for two section pipe with a positive pseudo reflection coefficient and parameter sets: a) $\bar{\zeta}_t = 3,\ \eta_t = 0.5$, b) $\bar{\zeta}_t = 3,\ \eta_t = 0.5$, c) $\bar{\zeta}_t = 9,\ \eta_t = 0.8$, d) $\bar{\zeta}_t = 9,\ \eta_t = 0.8$.

$$\bar{g}_i(\bar{s}) = \frac{1}{\sqrt{1+\frac{k_i}{\bar{s}t_*}}}\frac{\bar{g}_i^p(\bar{s})\sqrt{1+\frac{k_i}{\bar{s}t_*}} + \tanh\left(\bar{s}t_p\sqrt{1+\frac{k_i}{\bar{s}t_*}}\right)}{1+\bar{g}_i^p(\bar{s})\sqrt{1+\frac{k_i}{\bar{s}t_*}}\tanh\left(\bar{s}t_p\sqrt{1+\frac{k_i}{\bar{s}t_*}}\right)}. \tag{88}$$

These transfer functions are shown in Fig. 24, with $\bar{s} = \mathrm{j}\varpi$. With these drill string transfer functions, we derive the characteristic function $\bar{G}(\bar{s})$ of (43):

$$\bar{G}(\bar{s}) = \bar{g}_a(\bar{s})\frac{\bar{K}_a}{\bar{s}}\left(1-e^{-\bar{s}/\bar{\Omega}}\right) - \bar{g}_t(\bar{s})\frac{\bar{K}_t}{\bar{s}}\left(1-e^{-\bar{s}/\bar{\Omega}}\right). \tag{89}$$

We can now graphically evaluate the stability of the system by using the Nyquist criterion, see Theorem 1. The considered case is shown in a logarithmic Nyquist diagram in Fig. 25, where the original case considered was with 90 RPM as imposed angular velocity. We see that this system is unstable with a gain margin violation of ∼12 dB, which is very close to the 10 dB which was concluded from the axial stability map. This instability is hence clearly due to a resonance in the axial loop. Furthermore, we see that the severity of the instability can be reduced by increasing the rotation-rate to 135 RPM, corresponding to $\bar{\Omega} \approx 3.5$, as can also bee seen from the axial stability map. However, increasing the RPM even further (to 225 RPM) does not help but exacerbates the instability, as can also be seen in the axial stability map.

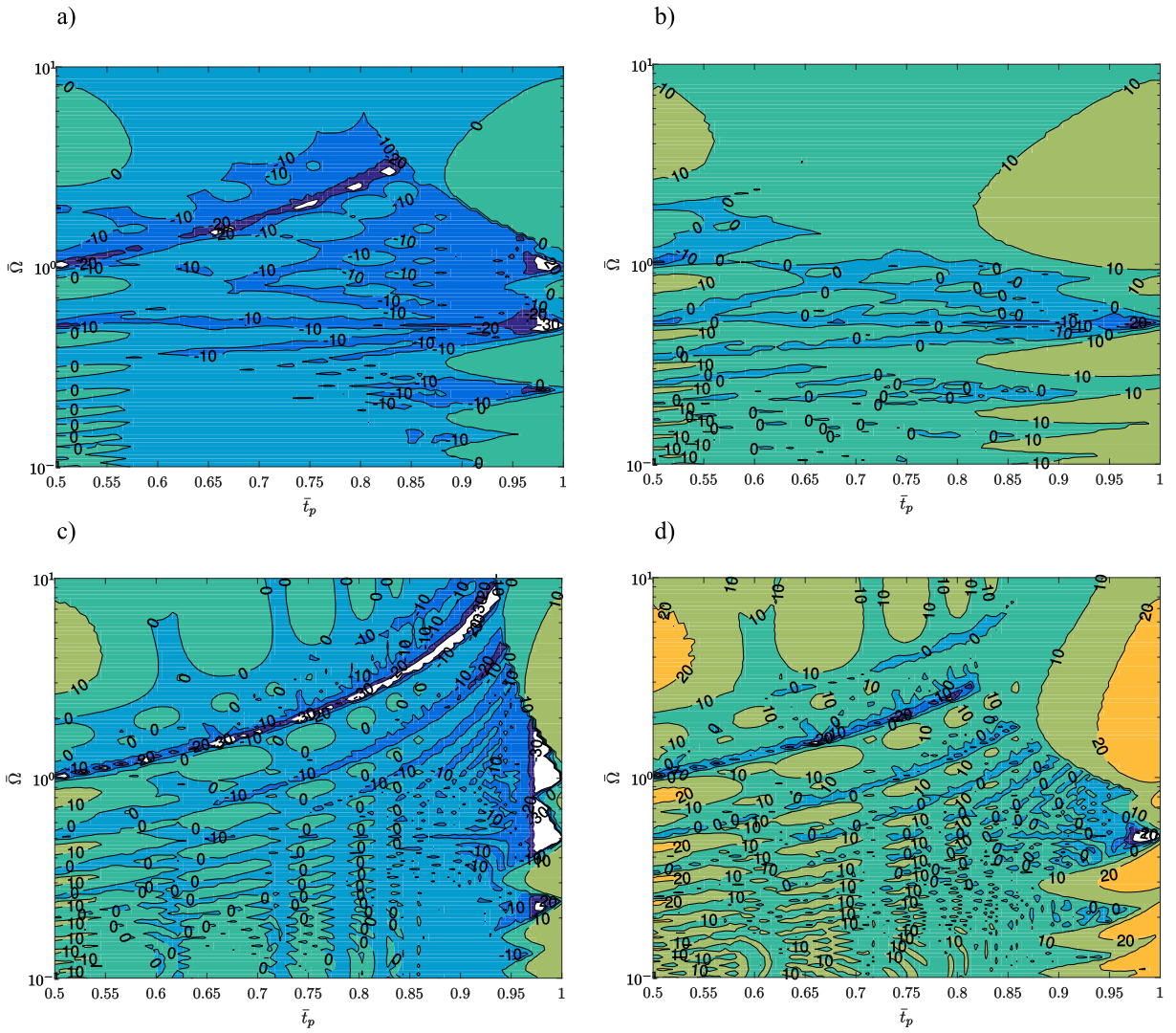

Fig. 23. Torsional loop transfer function normalized inverse gain margin, $M_{G,t}$ in dB, maps for two section pipe with a negative pseudo reflection coefficient and parameter sets: a) $\overline{\zeta}_t = 3,\ \eta_t = -0.5$, b) $\overline{\zeta}_t = 3,\ \eta_t = -0.5$, c) $\overline{\zeta}_t = 9,\ \eta_t = -0.8$, d) $\overline{\zeta}_t = 9,\ \eta_t = -0.8$.

6.4. Comparison with lumped model

Using the same example, we can also derive the transfer functions of the lumped RGD model [12,35]. Using the model from Table 1 in non-dimensional form:

$$\overline{g}_a(\bar{s}) = \frac{\zeta_a^c}{M}\frac{t_*}{\bar{s}} \tag{90}$$

$$\overline{g}_t(\bar{s}) = \frac{\zeta_t^c}{I}\frac{\bar{s}/t_*}{\frac{\bar{s}^2}{t_*^2} + \frac{C_t}{I}}, \tag{91}$$

where $M = A^c L^c \rho, I = I^c L^c \rho$, and the spring constant was fitted to match the first torsional resonance: $C_t = 650$. This yields the lumped transfer functions shown in Fig. 26. From this figure it is clear that the lumped RGD model is not an amenable representation for the considered example parameter set. In particular, the model only captures one of the drill string resonances, which are critical for determining system stability.

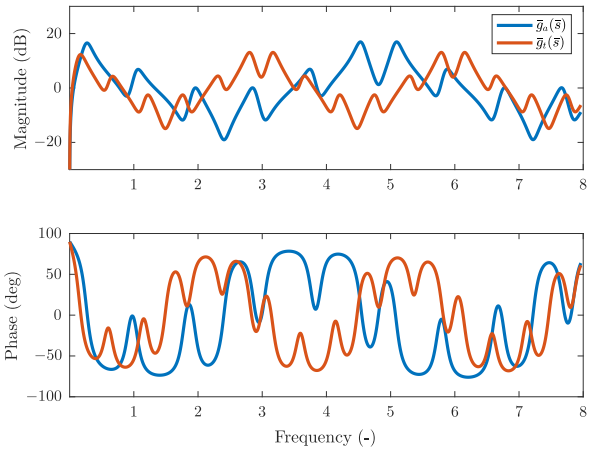

Fig. 24. Drill string transfer functions for the example case.

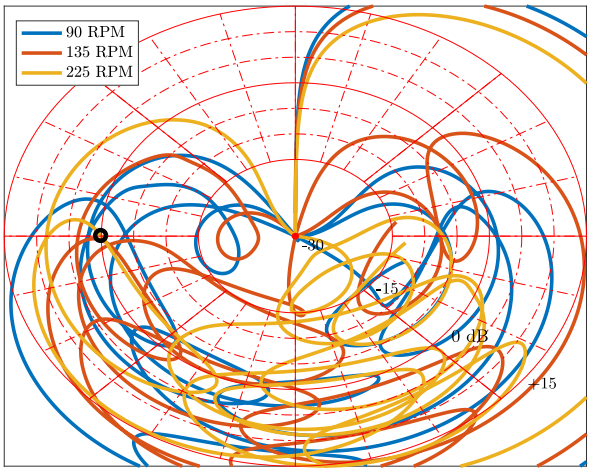

Fig. 25. Logarithmic Nyquist diagram for the characteristic function $\overline{G}(\overline{s})$ for the example case.

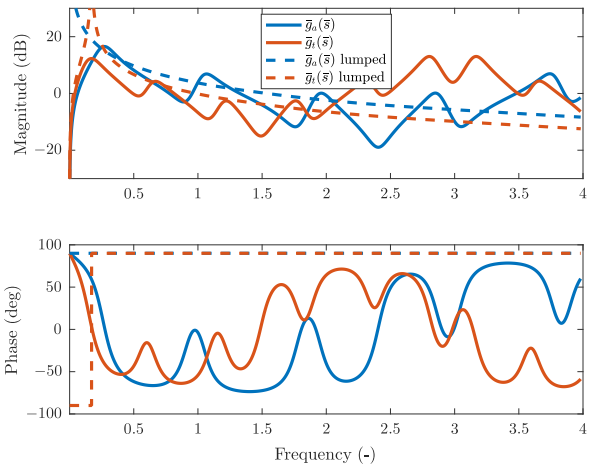

Fig. 26. Drill string transfer functions compared to with the lumped transfer functions for the example case.

7. Conclusions

In this paper we have characterized the linearized axial–torsional dynamics of a distributed drill string system in a minimal set of 5 parameters for the single section drill string and 8 parameters for the two-section drill string. For the single section drill-string these parameters are

1. $\overline{\Omega} = \frac{t_* N}{2\pi}\overline{\omega}$ - Dimensionless top-drive RPM, given as angular velocity relative to the drill string travel time. Determines the nominal delay in the bit rock interaction delay term.
2. $\overline{K}_a = K_a t_*$ - Nominal axial loop gain coefficient, determined by bit-rock interaction and drill string parameters.
3. $\overline{K}_t = K_t t_*$ - Nominal torsional loop gain coefficient, determined by bit-rock interaction and drill string parameters, and the axial to angular velocity ratio.
4. η_a - Pseudo reflection coefficient, given by the amount of damping of the axial dynamics.
5. η_t - Pseudo reflection coefficient, given by the amount of damping of the torsional dynamics.

For a two-section drill string, the following parameters are required in addition.

1. $\overline{\zeta}_a = \frac{\zeta_a^c}{\zeta_a^p}$: Approximately equals relative size of collar to pipe cross sectional area.
2. $\overline{\zeta}_t = \frac{\zeta_t^c}{\zeta_t^p}$: Approximately equals relative size of collar to pipe polar moment of inertia.
3. $\overline{t}_p = \frac{t_t^p}{t_t^p + t_t^c} \in [0, 1]$: drill pipe travel time relative to total drill string travel time.

Using these parameters we obtained sufficient conditions for stability of the isolated axial and torsional loop (note that this does not necessarily entail stability for the complete system).

The exact limit of stability is given by a significantly more complex relation and, as such, has been presented by a series of stability maps spanning the range of realistic physical parameters for the system. This analysis reveals complex dynamics for the distributed system. The main trends that emerges, however, is that a decrease in the inverse gain margin (leading to a more stable system) is obtained by decreasing the reflection coefficient and increasing RPM. These effect are also recognized in stated sufficient conditions for stability. A negative reflection coefficient (corresponding to a soft top-drive) is in many cases preferable to a positive reflection coefficient (corresponding to a stiff top-drive). Still, in particular for the axial dynamics, achieving stability can be difficult to achieve in practice due to the restrictions on RPM and the challenges of reducing the reflection coefficient through impedance matching.

We stress that the presented results illustrate the limitations of a low-order lumped-parameter model approach, in that multiple axial and torsional modes can be unstable and contribute to the overall system behavior.

The presented results also enable a more structured approach to analyzing non-local (non-linear) dynamics through the derivation of the minimal set of characteristic parameters. Moreover, the stability maps enables an effective test of accuracy of a transient simulation model. Using the developments in the present paper, a comprehensive simulation study of the non-local dynamics will be pursued in future work.

Acknowledgment

This work was supported by the Research Council of Norway, ConocoPhillips, Det norske oljeselskap, Lundin, Statoil and Wintershall through the research center DrillWell (203525/O30) at IRIS.

Appendix A. Accuracy of the delay model approximation

To evaluate the accuracy of the approximation utilized in Section 3.1 we compare the transfer function of the original wave equation with that of the approximation.

We assume that $Z_i^L = \infty \Rightarrow k_i^L = -1$ (which corresponds to a stiff top-drive with a velocity not affected by the force acting on it), which corresponds to a worst case for the approximation as in this case all the damping is in the domain where the approximation was performed, cf. (25), (26). The Laplace transform of the approximation model in (33) yields the transfer function $\hat{g}_i(s)$ given as

$$\hat{g}_i(s) = \frac{1 - e^{-2k_i t_i} e^{-s2t_i}}{1 + e^{-2k_i t_i} e^{-s2t_i}} = \frac{1 - \eta_i e^{-s2t_i}}{1 + \eta_i e^{-s2t_i}}, \quad i \in \{a, t\}. \tag{A.1}$$

Recalling that we have also defined the relation $\frac{V_b}{W_b}(s) = -\frac{1}{\zeta_a} g_a(s)$, for the original model, we can compare with the exact solution

from (9):

$$g_i(s) = \frac{1}{\sqrt{1+\frac{k_i}{s}}} \frac{1-e^{-s2t_i\sqrt{1+\frac{k_i}{s}}}}{1+e^{-s2t_i\sqrt{1+\frac{k_i}{s}}}}. \tag{A.2}$$

The transfer functions $\hat{g}_i(s)$ and $g_i(s)$ are compared in a Bode plot in Fig. A.27. This figure confirms the high accuracy of the delay-based model approximation of the distributed drill string dynamics and yields some interesting insights. In particular, we can obtain the magnitude of the (anti-) resonances by noting that these occur when denominator (numerator) of the transfer function is close to zero, i.e., when $s = \mathrm{j}\omega = \frac{\mathrm{j}\pi}{2t_i}k, \quad k = 1, 2\ldots$, at which point, we have $g_i(s = \frac{\mathrm{j}\pi}{2t_i}) \approx \frac{1\pm\eta_i}{1\mp\eta_i}$, and are hence only determined by $\eta_i = -k_i^d k_i^L$, i.e., by the in-domain damping and the coupling at the top-side boundary condition.

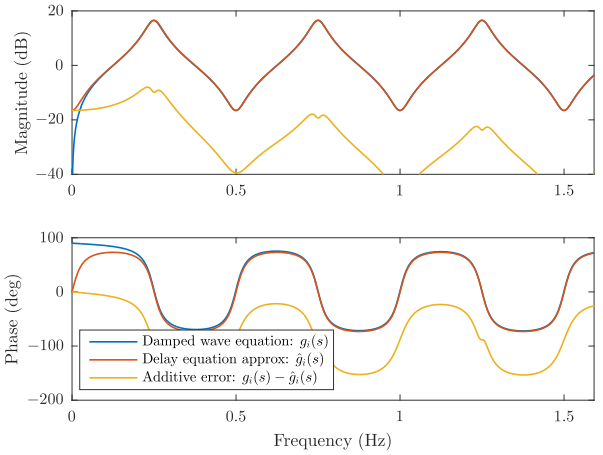

Fig. A.27. Bode plot showing the comparison of $g_i(s)$, in (A.2), with the approximation $\hat{g}_i(s)$, in (A.1), and the resulting additive error. Parameter values used are $k_i = 0.3\ \mathrm{s}^{-1}$ and $t_i = 1$ s. The comparison is valid for both $i = t, a$.

Appendix B. RGD axial model as a limiting case of the distributed model

Consider the distributed model of a two-section drill string with the axial transfer function

$$\frac{V_b}{W_b} = -\frac{1}{\zeta_a^c} g_a^c(s) = -\frac{1}{\zeta_a^c} \frac{g_a^p(s)\zeta_a^c + \zeta_a^p \tanh s\frac{t^c}{\bar{c}}}{\zeta_a^p + \zeta_a^c g_a^p(s)\tanh s\frac{t^c}{\bar{c}}}, \tag{B.1}$$

where, see Fig. 2 for notation,

$$-\frac{1}{\zeta_a^p} g_a^p(s) = \frac{V_p}{W_p} = -\frac{1}{Z_a^p} \frac{Z_a^p + Z_a^L \tanh s\frac{t^p}{\bar{c}}}{Z_a^L + Z_a^p \tanh s\frac{t^p}{\bar{c}}}. \tag{B.2}$$

Denote the mass of the collar section by M, which entails

$$M = L^c \rho A^c = L^c \frac{\zeta_a^c}{c_a}. \tag{B.3}$$

Assume that the collar section is infinitely *dense* and *short*, that is, we write $L^c = \frac{Mc_a}{\zeta_a^c} \equiv \xi$, and consider the limit

$$\lim_{\xi\to 0} \frac{V_b}{W_b} = \lim_{\xi\to 0} -\frac{\xi}{Mc_a} \frac{g_a^p(s)\frac{Mc_a}{\xi} + \zeta_a^p \tanh s\xi/c_a}{\zeta_a^p + \frac{Mc_a}{\xi} g_a^p(s)\tanh s\xi/c_a} = -\frac{1}{\zeta_a^p} \frac{1}{\frac{1}{g_a^p(s)} + \frac{M}{\zeta_a^p}s}, \tag{B.4}$$

where we have used the identity (easily obtained from a series expansion)

$$\lim_{\xi\to 0} \frac{\tanh \xi s/c_a}{\xi} = s/c_a. \tag{B.5}$$

The magnitude of the drill pipe transfer function can be assumed to be bounded away from zero: $|g_a^p(s)| > \epsilon > 0$ (corresponds to $|\eta_a| < 1$ which will always be true for realistic drill strings). Consequently, as the collar mass M becomes large, and collar length L^c becomes short, we obtain the limit

$$\lim_{\xi \to 0, M \to \infty} \frac{V_b}{W_b} \to \frac{1}{Ms}, \tag{B.6}$$

which is equivalent with the axial dynamics of the RGD model.

Summarizing the distributed two sectioned model corresponds to the RGD model only in the limit for a very large, but very short, collar section.

A similar analysis can be performed for the torsional dynamics of the RGD model, as well as for the axial and torsional dynamics of [16,18], see the Appendix of [22] for details.

Appendix C. Derivation of resonance characteristics of the two section drill string

Appendix C.1. Resonance frequencies

In this section, we will derive relations for the locations of the resonances and anti-resonances of the two-section drill-string derived in Section 2.2. Since the location the resonances are independent of the amount of dissipation in the system, we assume $k_i = 0$ and $Z_i^L = \infty$ to simplify the derivation. Recall from Section 3.1 that this means that the delay approximation is valid and from (5), (6), that:

$$\Gamma_i^c = t_i^c s, \quad \Gamma_i^p = t_i^p s, \quad Z_i^c = \zeta_i^c, \quad Z_i^p = \zeta_i^p, \tag{C.1}$$

where $t_i^c, t_i^p, \quad i \in \{a, t\}$, are the wave travel times for the two sections and ζ_i^c, ζ_i^p are given by the physical properties of the string. Denoting the response relation at location p, see Fig. 2, as $\frac{1}{\zeta_i^p} g_i^p(s)$, where with infinite load we have $g_i^p(s) = \tanh\ \Gamma_i^p = \tanh\ t_i^p s$, this enters in a two-port series configuration as the inverse load of the collar section such that the complete drill string response function is given by

$$\frac{V_b}{W_b}(s) \equiv \frac{-1}{\zeta_a^c} g_a(s), \quad \frac{\Omega_b}{T_b}(s) \equiv \frac{-1}{\zeta_t^c} g_t(s), \quad \text{where} \quad g_i(s) = \frac{\frac{\zeta_i^c}{\zeta_i^c} g_i^p(s) + \tanh t_i^c s}{1 + \frac{\zeta_i^c}{\zeta_i^p} g_i^p(s) \tanh t_i^c s}, \quad i \in \{t, a\}. \tag{C.2}$$

Denote the relative magnitude of the characteristic impedances as $\overline{\zeta}_i = \frac{\zeta_i^c}{\zeta_i^p}$ and insert for $g_i^p(s) = \tanh\ t_i^p s$ to obtain:

$$g_i(s) = \frac{\overline{\zeta}_i\ \tanh t_i^p s + \tanh t_i^c s}{1 + \overline{\zeta}_i \tanh t_i^p s \tanh t_i^c s}. \tag{C.3}$$

Evaluating $g_i^p(s)$ at $s = \mathrm{j}\omega$, we obtain

$$g_i(\mathrm{j}\omega) = \frac{\tanh(\mathrm{j}\omega t_i^p)\overline{\zeta}_i + \tanh(\mathrm{j}\omega t_i^c)}{1 + \overline{\zeta}_i\ \tanh(\mathrm{j}\omega t_i^p) \tanh(\mathrm{j}\omega t_i^c)} \tag{C.4}$$

$$= \frac{\mathrm{j}\tan(\omega t_i^p)\overline{\zeta}_i + \mathrm{j}\tan(\omega t_i^c)}{1 - \overline{\zeta}_i\ \tan(\omega t_i^p) \tan(\omega t_i^c)} \tag{C.5}$$

$$= \frac{-\mathrm{j}\overline{\zeta}_i\ \sin(\omega t_i^p)\cos(\omega t_i^c) - \mathrm{j}\cos(\omega t_i^p)\sin(\omega t_i^c)}{\overline{\zeta}_i\ \sin(\omega t_i^p)\sin(\omega t_i^c) - \cos(\omega t_i^p)\cos(\omega t_i^c)}, \tag{C.6}$$

where resonances and anti-resonances occur when the undamped denominator and numerator equals zero, respectively, i.e., with resonances at ω such that

$$\cos(t_i^p \omega)\cos(t_i^c \omega) - \overline{\zeta}_i \sin(t_i^p \omega)\sin(t_i^c \omega) = 0, \tag{C.7}$$

and anti-resonances at ω such that

$$\cos(t_i^p \omega)\sin(t_i^c \omega) + \overline{\zeta}_i \sin(t_i^p \omega)\cos(t_i^c \omega) = 0. \tag{C.8}$$

Example 1. Consider the case of $L^p = L^c$, i.e. $t_i^c = t_i^p$. Then, resonance frequencies are located at

$$\sin(t_i^p \omega)^2 - \overline{\zeta}_i \cos(t_i^p \omega)^2 = 0 \ \Rightarrow\ \omega = \frac{1}{t_i^p}\left(n\pi \pm \arctan(\sqrt{\overline{\zeta}_i})\right), \quad n = 0, 1, 2 \ldots, \tag{C.9}$$

and the anti-resonance frequencies

$$\sin(t_i^p\omega)\cos(t_i^p\omega) = 0 \;\Rightarrow\; \omega = \frac{n\pi}{2t_i^p}, \quad n = 0, 1, 2 \ldots . \tag{C.10}$$

Appendix C.2. Resonance magnitude

Next, we study the magnitude of the resonances in the two-section drill string. We will study two cases: first the case of impedance matching at the top-drive resulting in a rather agreeable expression, and then the more involved case of an unmatched load. These two can be considered as limiting cases where a real drilling system would be somewhere in between.

For the case of a matched load at the top of the pipe section p, we have $Z_i^L = Z_i^p$. For this case, the transfer function of this section reduces to $g_i^p(s) = \frac{\zeta_i^p}{Z_i^p} \approx 1$, and the full transfer function can be approximated by

$$g_i \approx g_m(s), \qquad g_m(s) = \frac{Z_i^c + Z_i^p \tanh\,\Gamma_i^c}{Z_i^p + Z_i^c \tanh\,\Gamma_i^c}. \tag{C.11}$$

Note that (C.11) equals the response of only the lowermost section, c, with a load equal to the characteristic impedance of the top-most section p. Hence, the result for the single section drill string given in Section 2.1.2 can be used, meaning that $g_m(s)$ is characterized by the travel time t_i^c and the reflection coefficient $\eta_i^c = \frac{\zeta_i^p - \zeta_i^c}{\zeta_i^p + \zeta_i^c} e^{-k_i^c t_i^c}$, with bounds as given in (39).

For cases where the load at the top-drive is not matched to pipe impedance, the resonance frequencies are dependent on a more complex interaction between the two sections, as was shown in Section Appendix C.1. However, by studying the Bode plots of a wide range of parameter sets, the gain at the resonant peaks of the full drill string transfer function seems to satisfy the bound[3]:

$$|g_i(s)| \le |g_m(s)| \frac{1+|\eta_i|}{1-|\eta_i|} \le \frac{1+|\eta_i^c|}{1-|\eta_i^c|} \frac{1+|\eta_i|}{1-|\eta_i|}. \tag{C.12}$$

The first inequality comes from heuristically assuming that the magnitude of the response is a product of that of the two sections, and observing that it follows the general response of $g_m(s)$. The second inequality follows from the first and (39), which holds for $|g_m(s)|$. These bounds are illustrated in Fig. 6.

Appendix D. Derivation of explicit sufficient stability conditions

Proof of Proposition 1. *Consider the case of a single section drill string. The magnitude of the axial term $\overline{G}_a(\bar{s})$, as in (36), of the characteristic equation can be bounded according to*

$$|\overline{G}_a(\bar{s})| = \left| \overline{g}_a(\bar{s}) \frac{\overline{K}_a}{\bar{s}} \left(1 - e^{-\bar{s}/\overline{\Omega}}\right) \right| \le \left| \frac{1+|\eta_a|}{1-|\eta_a|} \frac{\overline{K}_a}{\bar{s}} 2 \right|, \tag{D.1}$$

*where we have used (39) for $i = a$ and the fact that $\left|(1 - e^{-s/\overline{\Omega}})\right| \le 2$. The bound (D.1) decreases for higher frequencies, due to the $\bar{s}$ in the denominator The lowest frequency at which **Cond. A1** (see (47) in Section 4.2) can be satisfied (cf. (55)) is $\varpi = \pi\overline{\Omega}$. At this frequency, we can obtain a bound on the magnitude, and hence a sufficient condition for stability, using **Cond. A2**:*

$$2\frac{1+|\eta_a|}{1-|\eta_a|}\frac{\overline{K}_a}{\overline{\Omega}\pi} < 1 \tag{D.2}$$

Detailing the characteristic quantities,

$$\overline{K}_a = \frac{a\zeta\epsilon N t_*}{\zeta_a}, \quad \overline{\Omega} = \frac{t_*}{t_N} = \frac{N\overline{\omega}}{2\pi} t_*, \tag{D.3}$$

(D.2) is equivalent with

$$\frac{1+|\eta_a|}{1-|\eta_a|}\frac{4}{\overline{\omega}}\frac{a\zeta\epsilon}{\zeta_a} < 1. \tag{D.4}$$

Proof of Proposition 2. *Consider a two sectioned drill-string. We use the bound from (40) $\overline{\zeta}_a > \frac{1+|\eta_a^c|}{1-|\eta_a^c|}$, combined with (C.12):*

$$|g_i| \le \frac{1+\eta_i}{1-\eta_i}\overline{\zeta}_a \tag{D.5}$$

[3] We have not been able show this relation rigorously but have not yet observed cases where it has been incorrect.

then noting that $\frac{\overline{\zeta}_a}{\zeta_a^c} = \frac{1}{\zeta_a^p}$, *and that the the two section loop gain is* $\overline{K}_a = \frac{a\zeta\epsilon N t_*}{\zeta_a^c}$, *we follow the same procedure as in Proof of Proposition 1 and obtain the sufficient condition for stability:*

$$\frac{1+|\eta_a|}{1-|\eta_a|}\frac{4}{\overline{\omega}}\frac{a\zeta\epsilon}{\zeta_a^p} < 1. \tag{D.6}$$

Proof of Proposition 3. *Consider the case of a single section drill string. With* $\eta_t \geq 0$ *the first torsional resonance is located at* $\varpi_{r,1} = \frac{\pi}{2}$, *while with* $\eta_t < 0$ *the first torsional resonance is located at* $\varpi_{r,1} = \pi$, *see e.g. (38).*

At resonance, the drill string transfer function takes the magnitude $|\overline{g}_t(\mathrm{j}\varpi_{r,1})| \approx \frac{1+\eta_t}{1-\eta_t}$, *while the magnitude of the full torsional term of the characteristic equation is bounded by, for* $\eta_t \geq 0$:

$$|\overline{G}_t(\overline{s})|_{\overline{s}=\mathrm{j}\frac{\pi}{2}} = \left|\overline{g}_t(\overline{s})\frac{\overline{K}_t}{\overline{s}}\left(1-e^{-\overline{s}/\overline{\Omega}}\right)\right|_{\overline{s}=\mathrm{j}\frac{\pi}{2}} \leq 4\overline{K}_t\frac{1}{\pi}\frac{1+|\eta_t|}{1-|\eta_t|}, \tag{D.7}$$

where we again used the bound $\left|(1-e^{-s/\overline{\Omega}})\right| \leq 2$, *and hence a sufficient condition for stability of the torsional dynamics is, from* ***B2:***

$$4\overline{K}_t\frac{1}{\pi}\frac{1+|\eta_t|}{1-|\eta_t|} < 1. \tag{D.8}$$

Equivalently, for $\eta_t < 0$ *the dimensionless Laplace variable is evaluated at* $\overline{s} = \mathrm{j}\pi$ *and we obtain the sufficient conditions*

$$2\overline{K}_t\frac{1}{\pi}\frac{1+|\eta_t|}{1-|\eta_t|} < 1. \tag{D.9}$$

Proof of Proposition 4. *Consider a two sectioned drill-string. We use the bound from (40) for* $i = t$: $\overline{\zeta}_t > \frac{1+|\eta_t^c|}{1-|\eta_t^c|}$. *Combining with (C.12), as was done in Proof of Proposition 2, we obtain for the two-sectioned case with* $\eta_t \geq 0$ *the modified bound*

$$|\overline{G}_t(\overline{s})|_{\overline{s}=\mathrm{j}\frac{2\pi}{4}} = \left|\overline{g}_t(\overline{s})\frac{\overline{K}_t}{\overline{s}}\left(1-e^{-\overline{s}/\overline{\Omega}}\right)\right|_{\overline{s}=\mathrm{j}\frac{2\pi}{4}} \leq 4\overline{K}_t\frac{1}{\pi}\overline{\zeta}_t\frac{1+|\eta_t|}{1-|\eta_t|}. \tag{D.10}$$

Hence, a sufficient condition for stability is, from ***B2***:

$$4\overline{K}_t\frac{1}{\pi}\overline{\zeta}_t\frac{1+|\eta_t|}{1-|\eta_t|} < 1. \tag{D.11}$$

Equivalently, for $\eta_t < 0$ the resonance occurs at $\overline{s} = \mathrm{j}\pi$ and we obtain the stability bound

$$2\overline{K}_t\frac{1}{\pi}\overline{\zeta}_t\frac{1+|\eta_t|}{1-|\eta_t|} < 1. \tag{D.12}$$

Appendix D.1. Stability conditions as pertaining to the RGD model

It may be instructive to consider how the stability conditions derived in this paper relates to previous stability analyses for lumped-parameter models.

For the RGD model [12] we have that $\overline{K}_a = N\Psi$ (as stated in the non-dimensional formulation in Ref. [35]), and for the axial drill string transfer function, it holds that $g_a(s) = \frac{1}{s}$. From **A1** in (47):

$$|\arg\frac{\overline{K}_a}{s^2}\left(1-e^{-\mathrm{j}\varpi/\overline{\Omega}}\right)| = 180 \tag{D.13}$$

$$\Rightarrow\ |\arg\left(1-e^{-\mathrm{j}\varpi/\overline{\Omega}}\right)| = 0 \tag{D.14}$$

$$\Rightarrow\ \varpi = \pi\overline{\Omega} \tag{D.15}$$

From **A2**, in (48):

$$\left|\frac{\overline{K}_a}{s^2}\left(1-e^{-\mathrm{j}\pi}\right)\right|_{s=\mathrm{j}\pi\overline{\Omega}} > 1 \tag{D.16}$$

$$\Rightarrow\ \frac{2\overline{K}_a}{\overline{\Omega}^2\pi^2} > 1, \tag{D.17}$$

and consequently, inserting for $\overline{K}_a = N\Psi$, we obtain *instability* when

$$\frac{1}{\overline{\overline{\Omega}}} > \frac{\pi}{\sqrt{2N\Psi}}, \tag{D.18}$$

which is equivalent with

$$\overline{\Omega} < \sqrt{\frac{8\zeta\epsilon a}{NM}}. \tag{D.19}$$

References

[1] S. Jardine, D. Malone, M. Sheppard, Putting a damper on Drilling's bad vibrations, Oilfield Rev. 1 (January) (1994) 15–20.
[2] V. Dunayevsky, F. Abbassian, Application of stability approach to bit dynamics, SPE Drill. Complet. 13 (2) (1998) 22–25, https://doi.org/10.2118/30478-PA.
[3] J. Jansen, L. van den Steen, Active damping of self-excited torsional vibrations in oil well drillstrings, J. Sound Vib. 179 (4) (1995) 647–668, https://doi.org/10.1006/jsvi.1995.0042.
[4] A. Serrarens, M. van de Molengraft, J. Kok, L. van den Steen, H-infinity control for suppressing stick-slip in oil well drillstrings, IEEE Control Syst. Mag. 18 (2) (1998) 19–30, https://doi.org/10.1109/37.664652.
[5] Third International Colloquium on Nonlinear Dynamics and Control of Deep Drilling Systems, E. Detournay, D.V.N. van de Wouw, Y. Zhou (Eds.), Nonlinear Dynamics and Control of Deep Drilling Systems, 2014. Minneapolis.
[6] D.J. Runia, S. Dwars, I.P.J.M. Stulemeijer, A brief history of the Shell "Soft Torque Rotary System" and some recent case studies, in: SPE/IADC Drilling Conference, Society of Petroleum Engineers, 2013, pp. 69–76, https://doi.org/10.2118/163548-MS.
[7] C. Sagert, F. Di Meglio, M. Krstic, P. Rouchon, Backstepping and flatness approaches for stabilization of the stick-slip phenomenon for drilling, in: IFAC Proceedings Volumes (IFAC-PapersOnLine), 2013, pp. 779–784, https://doi.org/10.3182/20130204-3-FR-2033.00126.
[8] T. Vromen, N. van de Wouw, A. Doris, P. Astrid, H. Nijmeijer, Observer-based output-feedback control to eliminate torsional drill-string vibrations, in: 53rd IEEE Conference on Decision and Control, 2014, pp. 872–877, https://doi.org/10.1109/CDC.2014.7039491.
[9] J.-M. Godhavn, Drilling seeking automatic control solutions, in: B. Sergio (Ed.), 18th IFAC World Congress, Milano, Milano, Italy, 2011, pp. 10842–10850, https://doi.org/10.3182/20110828-6-IT-1002.00551.
[10] T. Vromen, C.-H. Dai, N. van de Wouw, T. Oomen, P. Astrid, H. Nijmeijer, Robust output-feedback control to eliminate stick-slip oscillations in drill-string systems, in: IFAC-PapersOnLine, vol. 48, Elsevier Ltd., 2015, pp. 266–271, https://doi.org/10.1016/j.ifacol.2015.08.042.
[11] J. de Bruin, A. Doris, N. van de Wouw, W. Heemels, H. Nijmeijer, Control of mechanical motion systems with non-collocation of actuation and friction: a Popov criterion approach for input-to-state stability and set-valued nonlinearities, Automatica 45 (2) (2009) 405–415, https://doi.org/10.1016/j.automatica.2008.09.008.
[12] T. Richard, C. Germay, E. Detournay, A simplified model to explore the root cause of stickâĂŞslip vibrations in drilling systems with drag bits, J. Sound Vib. 305 (3) (2007) 432–456, https://doi.org/10.1016/j.jsv.2007.04.015.
[13] T. Insperger, G. Stépán, J. Turi, State-dependent delay in regenerative turning processes, Nonlinear Dyn. 47 (1–3) (2006) 275–283, https://doi.org/10.1007/s11071-006-9068-2.
[14] S.A. Tobias, Machine Tool Vibration, Blakie, London, 1965.
[15] C. Germay, V. Denoël, E. Detournay, Multiple mode analysis of the self-excited vibrations of rotary drilling systems, J. Sound Vib. 325 (1–2) (2009) 362–381, https://doi.org/10.1016/j.jsv.2009.03.017.
[16] K. Nandakumar, M. Wiercigroch, Stability analysis of a state dependent delayed, coupled two DOF model of drill-string vibration, J. Sound Vib. 332 (10) (2013) 2575–2592, https://doi.org/10.1016/j.jsv.2012.12.020.
[17] Y. Nishimatsu, The mechanics of rock cutting, Int. J. Rock Mech. Min. Sci. 9 (February 1971) (1972) 261–270.
[18] B. Besselink, N. van de Wouw, H. Nijmeijer, A semi-analytical study of stick-slip oscillations in drilling systems, J. Comput. Nonlinear Dyn. 6 (2) (2011) 021006, https://doi.org/10.1115/1.4002386.
[19] C. Germay, N. van de Wouw, H. Nijmeijer, R. Sepulchre, Nonlinear drillstring dynamics analysis, SIAM J. Appl. Dyn. Syst. 8 (2) (2009) 527–553, https://doi.org/10.1137/060675848.
[20] A.S. Yigit, A.P. Christoforou, Stick-slip and bit-bounce interaction in oil-well drillstrings, J. Energy Resour. Technol. (2006), https://doi.org/10.1115/1.2358141.
[21] B. Besselink, T. Vromen, N. Kremers, N. van de Wouw, Analysis and control of stick-slip oscillations in drilling systems, IEEE Trans. Control Syst. Technol. 24 (1) (2016) 226–239, https://doi.org/10.1109/TCST.2015.2502898.
[22] U.J.F. Aarsnes, O.M. Aamo, Linear stability analysis of self-excited vibrations in drilling using an infinite dimensional model, J. Sound Vib. 360 (2016) 239–259, https://doi.org/10.1016/j.jsv.2015.09.017.
[23] P.E. Pastusek, D. Ertas, L. Wang, J.R. Bailey, Drillstring mechanics model for surveillance, root cause analysis, and mitigation of torsional and axial vibrations, in: Proceedings of 2013 SPE/IADC Drilling Conference and Exhibition (December), 2013, https://doi.org/10.2118/163420-MS.
[24] M. Ertas, E. Biediger, S. Sundararaman, J. Bailey, V. Gupta, N.-R. Bangaru, S. Bangaru, Methods and Systems for Mitigating Drilling Vibrations, 2009.
[25] R.J. Shor, M.W. Dykstra, O.J. Hoffmann, M. Coming, For better or worse: applications of the transfer matrix approach for analyzing axial and torsional vibration, in: SPE/IADC Drilling Conference and Exhibition, 2015, https://doi.org/10.2118/173121-MS.
[26] F. Di Meglio, U.J.F. Aarsnes, A distributed parameter systems view of control problems in drilling, IFAC-PapersOnLine 48 (6) (2015) 272–278, https://doi.org/10.1016/j.ifacol.2015.08.043.
[27] J. Stecki, D. Davis, Fluid transmission lines distributed parameter models part 1: a review of the state of the art, Proc. Inst. Mech. Eng. Part A: J. Power Energy 200 (4) (1986) 215–228.
[28] R.E. Goodson, R.G. Leonard, A survey of modeling techniques for fluid line transients, J. Basic Eng. 94 (2) (1972) 474, https://doi.org/10.1115/1.3425453.
[29] S. Dwars, Recent advances in soft torque rotary systems, in: Proceedings of 2015 SPE/IADC Drilling Conference, No. March, 2015, pp. 17–19, https://doi.org/10.2118/173037-MS. London, United Kingdom.
[30] T. Richard, C. Germay, E. Detournay, Self-excited stickâĂŞslip oscillations of drill bits, Comptes Rendus Mécanique 332 (8) (2004) 619–626, https://doi.org/10.1016/j.crme.2004.01.016.
[31] R. Courant, D. Hilbert, Methods of Mathematical Physics, CUP Archive, 1965.
[32] U.J.F. Aarsnes, M.S. Gleditsch, O.M. Aamo, A. Pavlov, Modeling and avoidance of heave-induced resonances in offshore drilling, SPE Drill. Complet. 29 (04) (2014) 454–464, https://doi.org/10.2118/173178-PA.
[33] E. Detournay, T. Richard, M. Shepherd, Drilling response of drag bits: theory and experiment, Int. J. Rock Mech. Min. Sci. 45 (8) (2008) 1347–1360, https://doi.org/10.1016/j.ijrmms.2008.01.010.
[34] T. Richard, F. Dagrain, E. Poyol, E. Detournay, Rock strength determination from scratch tests, Eng. Geol. 147 (October) (2012) 91–100, https://doi.org/10.1016/j.enggeo.2012.07.011.
[35] A. Depouhon, E. Detournay, Instability regimes and self-excited vibrations in deep drilling systems, J. Sound Vib. 333 (7) (2014) 2019–2039, https://doi.org/10.1016/j.jsv.2013.10.005.

[36] R.F. Curtain, H. Zwart, An Introduction to Infinite-dimensional Linear Systems Theory, Texts in Applied Mathematics, vol. 21, Springer New York, New York, NY, 1995, https://doi.org/10.1007/978-1-4612-4224-6.
[37] T. Vromen, N. van de Wouw, A. Doris, P. Astrid, H. Nijmeijer, Nonlinear output-feedback control of torsional vibrations in drilling systems, Int. J. Robust Nonlinear Control 18 (October 2014) (2017) 557–569, https://doi.org/10.1002/rnc.3759, arXiv:arXiv:1505.02595v1.
[38] K.J. Åström, R.M. Murray, Feedback Systems: an Introduction for Scientists and Engineers, second ed., Princeton University Press, 2010.